Numerical Simulation of Nanofluid Cooling in a Single-Cylinder Diesel Engine

Master`s thesis in Energy – Thermal Machines

Lukas Brayn Bøthun

University of Bergen

Geophysical Institute

Western Norway University of Applied Sciences

Department of Mechanical and Marine Engineering

Bergen, 1. June 2023

Numerical Simulation of Nanofluid Cooling in a Single-Cylinder Diesel Engine

Lukas Brayn Bøthun

University of Bergen (UIB)
Faculty of Mathematics and Natural Sciences
Geophysical Institute
5020 Bergen, Norway

In cooperation with:
Western Norway University of Applied Sciences (HVL)
Faculty of Engineering and Science
Department of Mechanical and Marine Engineering
5020 Bergen, Norway

Norwegian title:	Numerisk Simulering av Nanofluid Kjøling I en èn-sylindret Diesel Motor
Author, student number HVL/UIB:	Lukas Brayn Bøthun, 576344 / 304291
Study program:	Energy Technology, Thermal Machines
Date:	01.06.23
Main supervisor:	Boris Balakin
Co-supervisor:	Peter Edgar Koch

Acknowledgements

This thesis represents the final step of a two-year master's program in energy technology with specialization in thermal machines. The program is a cooperation between the University of Bergen (UIB) and Western Norway University of Applied Sciences (HVL) where this report accounts for 30 of 120 credits.

I would like to thank my supervisor at Boris Balakin for all his help and guidance through the whole project, which has given me a lot of knowledge about computational fluid dynamics and nanofluids. I would also like to thank Peter Edgar Koch, coordinator for the specialization in thermal machines, for a well-executed master's program and guidance through these two years.

Finally, I want to thank my fellow students in the study program for making these last years more fun than they would have been without them.

Lukas Bøthun

Bergen 1. June 2023

Abstract

The objective of this thesis is to investigate the change in an engine`s thermal field and heat transfer when using nanofluid instead of water as coolant. The project is done on a single-cylinder diesel engine and numerical simulation software is used to determine the temperature distribution of the solid parts. The engine is installed in the laboratory at Western Norway University of Applied Science and is used as a research engine. The engine was disassembled to create an accurate 3D model of the parts including the cooling channels. A 1D engine simulation was used to predict the in-cylinder heat transfer to the coolant at a certain engine load. The heat transfer is used further as a heat source boundary condition for the CFD simulation. Three different nanofluids were tested and water was used as coolant in a reference simulation for comparison. Two of the nanofluids are water-based with a concentration of 2.5 and 10 weight percent carbon black nanoparticles with a size of 50 nm. The third nanofluid is water-based with a volume concentration of 2 % 150 nm aluminum oxide nanoparticles. The results from the CFD simulations show that the average and maximum temperatures on selected engine surfaces are slightly higher with the carbon black nanofluids compared to the reference simulation, indicating a lower heat transfer coefficient. However, the aluminum oxide nanofluid resulted in slightly lower surface temperatures compared to the reference simulation, indicating improved heat transfer. The findings suggest that the increase in viscosity of the nanofluids negates the increased thermal conductivity which was expected to enhance the heat transfer.

Table of Content

List of Figures

List of Tables

1. Introduction

The internal combustion engine is still by far the most dominant power conversion technology used in the global transportation sector, even though alternative technologies are becoming increasingly popular. Maritime vessels and heavy-duty vehicles will likely use the combustion engine for many decades to come.

Chemical energy in a fuel is converted to thermal energy during combustion in the internal combustion engine. Some of the thermal energy is converted to useful mechanical work and the rest leaves the system as heat dissipated to the surroundings. Fuels based on hydrocarbons are almost exclusively used today, and thereby releasing large amounts of CO_2 into the atmosphere which is undesired. However, a range of environmental and climate-friendly fuels are also suitable for the combustion engine, including biofuels, ammonia, and hydrogen. The fuel flexibility ensures that the combustion engine has an important place in the future transportation and energy system.

Development of energy effective products is of high importance due to the ongoing challenges with climate change and energy supply. Increasing the efficiency enables the same amount of work to be done while using less energy, and possibly reduce some emissions as well. In the internal combustion engine, energy is dissipated to the atmosphere through the coolant, lube oil, and exhaust gasses, which are pure losses and should be reduced to increase efficiency. However, the temperature of engine components must be within reasonable limits to ensure reliability and engine performance. To avoid overheating of the engine components, excess energy must be rejected in a timely manner. A coolant jacket around the combustion chamber, valves and cylinder head usually ensures that temperatures are kept within desired limits.

Operation of the engine's cooling system is also a source of energy loss. A pump is required to force the coolant through the engine components and a radiator or heat exchanger is needed to dissipate the energy to the atmosphere. The radiator is a source of drag on a car and increases the energy needed to keep the car moving. Increasing the coolant heat transfer properties can make it possible to reduce the coolant flow rate and the pumping power required while

maintaining the desired heat transfer. The physical size and weight of the heat exchanger used to dissipate excess energy can also be reduced.

There are generally two methods to optimize the coolant side heat transfer, one is to improve the geometry and the other is to improve the coolant properties, with the latter being examined in this thesis. The coolant properties will be changed by using a nanofluid coolant, which is a fluid that contain particles of nanometer size, and thereby increasing the fluid heat transfer properties. Nanofluid coolant in combustion engines has the potential to increase the effectiveness of the cooling system significantly [1].

To quantify the improvements, it is essential to obtain an accurate overview of the temperature distribution in the engine. One method to obtain the heat flux and temperature distribution is through extensive instrumentation of the engine, which is not practical in many settings. Another method, which is often preferred, is to use numerical simulation software. Computational Fluid Dynamics (CFD) and Conjugate Heat Transfer (CHT) models are effective at determining the interaction between the cooling circuit and the solid regions of the engine. The thermal distribution in the engine components depends on the effectiveness of the cooling system and on the applied thermal load. When the thermal load and cooling system conditions are modelled correctly, the thermal field of the engine should match the experimental one [2].

1.1. Project Description and Objectives

The objective of this thesis is to investigate the change in an engine`s thermal field and heat transfer when using nanofluid instead of water as coolant. The project is done on a single-cylinder diesel engine and numerical simulation software is used to determine the temperature distribution. If the nanofluid simulations show improved heat transfer characteristics by reducing the surface temperatures, then it will be determined how much the coolant flow rate can be reduced while still achieving the same temperatures as seen in the reference simulation. The results can serve as a basis for future experimental testing and optimization of the engine. This research also aims to increase the knowledge about the use of nanofluid coolant in engines by performing an analysis with a specific example.

The main objectives for the project are listed below.

- Create a 3D model of the engine with internal cooling channels.
- Determine heat transfer from combustion chamber to the cylinder head and liner.
- Determine cooling water boundary conditions.
- Create reference CFD simulation with water as coolant.
- Determine nanofluid properties and simulation method.
- Create CFD simulation with nanofluid as coolant.
- Evaluate results from the reference and nanofluid simulation.

2. Theory

Fluid dynamics describe the motion of fluids, were a fluid can be a gas or a liquid and heat transfer is about the exchange of heat energy between objects. This chapter will explain some basic concepts within fluid dynamics and heat transfer that are needed to understand the methodology and results.

2.1. Fluid Dynamics

The governing equations of fluid dynamics are built upon three principals:

- *Conservation of mass*
- *Conservation of energy*
- *Conservation of momentum*

Conservation of mass is described by the continuity equation and is shown in equation (1), where $\boldsymbol{V}$ is the flow velocity vector. The equation states that for an incompressible fluid, the mass flow rate into a given volume is equal to the mass flow rate out of the same volume.

$$\nabla \boldsymbol{V} = 0 \tag{1}$$

The Navier-Stokes equation is derived from the conservation of momentum principle and is based on Newtons second law of motion ($\boldsymbol{F} = m\boldsymbol{a}$) applied to a fluid element. A simplified version of the Navier-Stokes equation is shown in equation (2). Where ν is the kinematic viscosity of the fluid and ρ is the density. The equation is valid for a steady flow of an incompressible Newtonian fluid without free surface.

$$(\boldsymbol{V} \cdot \nabla)\boldsymbol{V} = -\frac{1}{\rho}\nabla P + \nu \nabla^2 \boldsymbol{V} \tag{2}$$

The left side of the equation represents the acceleration of a fluid element through a velocity field. The first part of the right-hand side describes the pressure forces acting on the element and the second part describes the viscous forces. The equation states that the change of momentum in a fluid element is equal to the sum of forces acting on the element.

When heat transfer or energy conversion is part of the problem, an additional equation is needed. The energy equation is based on the principle of conservation of energy, also known as the first law of thermodynamics, which states that *energy can neither be created or destroyed during a process, it can only change forms*. The energy equation states that the change of internal energy in a fluid element is equal to the sum of energy being added or removed from the element. A simplified energy equation for incompressible flow is shown in equation (3), where ρ is the density, c_p is the specific heat capacity, T is the temperature, k is the fluid conductivity and Φ represents dissipation.

$$\rho c_p \left[\frac{\partial T}{\partial t} + (\boldsymbol{V} \cdot \nabla)T\right] = k\nabla^2 T + \Phi \tag{3}$$

2.1.1. Laminar and Turbulent Flows

Laminar flow occurs at low flow velocities and can be described as fluid particles flowing in parallel layers without mixing. Higher flow velocities will make the fluid particles move across the parallel layers and mixing of the layers will occur, this type of flow is called turbulent. Turbulent flow is a non-stationary and chaotic type of flow that consists of swirls called eddies. Large eddies transfer energy to smaller eddies, which again transfer energy to even smaller eddies. Eventually when the eddy currents get small enough, they will dissipate into heat due to viscous forces in the fluid.

The transition from laminar to turbulent flow depends on several factors, including the geometry, surface roughness, temperature, and the type of fluid [3]. A method to evaluate if a fluid flow is laminar or turbulent is the Reynolds number (Re), which is a dimensionless number shown in equation (4). Where ρ represent the density of the fluid, v is the flow velocity and L is a characteristic length, which can be the diameter of a pipe or the depth of a channel. The dynamic viscosity of the fluid is represented by μ.

$$Re = \frac{\rho v L}{\mu} \tag{4}$$

The Reynolds number describes the ratio of inertial forces to the viscous forces in the fluid. Reynolds determined, based on experiments, that for a circular pipe flow turbulent flow would happen with Re > 4000 and laminar flow would happen with Re < 2000. The range in-between indicates a transition phase. However, the Reynolds transition number between laminar and turbulent flow can vary greatly depending on the geometry, surface roughness and fluid properties [4].

The chaotic nature of turbulent flows makes them hard to model exactly. A wide variety of different methods are available to describe the turbulent flow. The most accurate method is direct numerical simulation (DNS) which resolves all scales of turbulence without the use of a turbulence model. However, this method requires substantial computational power and is not practical for normal applications.

The most often used method to model turbulence is with Reynolds Averaged Navier-Stokes (RANS), which is a mathematical approach to solve the governing equations of fluid flow. The approach assumes that the flow variables can be decomposed into a time averaged $\bar{\phi}$ and a fluctuating ϕ' component as in equation (5). Where ϕ can represent velocity, pressure, or energy [5].

$$\phi = \bar{\phi} + \phi' \tag{5}$$

The time averaged component is assumed to be steady, and the fluctuating component is assumed to be turbulent and is described using turbulence models. The turbulence models in RANS are based on the concept of eddy viscosity and the most commonly used turbulence models in RANS are the K-epsilon and Reynolds stress models. But even though it is a common method to model turbulence, RANS has its limitations. It cannot capture the details of turbulent flow accurately, such as the formation and dissipation of turbulent eddies. This is because RANS models are based on statistical averaging and cannot resolve the details of individual eddies. RANS is also dependent on turbulence models that must be suitable for the specific situation, and the use of an unsuitable turbulence model can introduce significant errors in the results [6].

2.1.2. Wall Treatment

The effect of fluid flow interaction with the walls is important in flow modeling, especially in heat transfer problems. The turbulent boundary layer, which is the part of the fluid flow influenced by the presence of the wall, can be divided into three regions: The *viscous sublayer, buffer layer* and the *log-law layer* [3]. A velocity profile of the turbulent boundary layer with the three regions is illustrated in Figure 1.

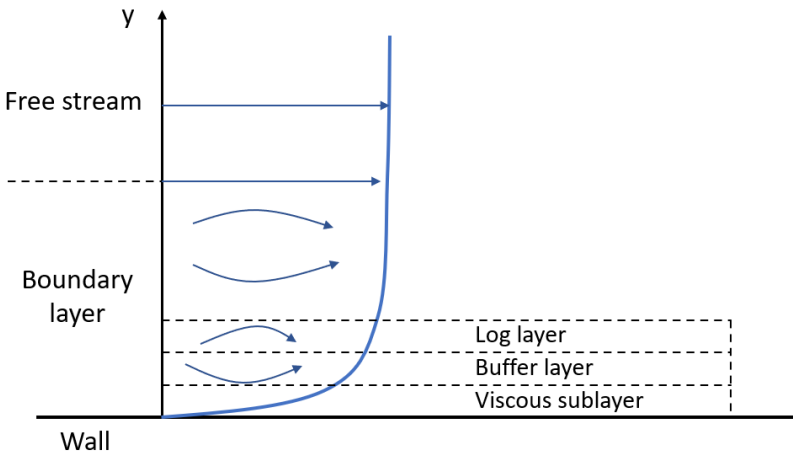

Figure 1 Velocity profile of a turbulent boundary layer [7]

The thickness of each region can be described by the non-dimensional wall distance parameter y^+, which is a measure of the distance of the first computational cell adjacent to the wall in relation to the wall's boundary layer. y^+ is calculated using equation (6), with y representing the distance from the wall to the center of the first cell and u_τ is the friction velocity [3].

$$y^+ = \frac{y\rho u_\tau}{\mu} \tag{6}$$

Another important parameter in turbulent flows is u^+, which is a non-dimensional velocity that characterizes the velocity profile near the walls. u^+ is calculated by equation (7) , where U is the local velocity at a certain distance from the wall.

$$u^+ = \frac{U}{u_\tau} \tag{7}$$

The viscous sublayer is the part of the fluid in proximity and in contact with the wall. The layer is dominated by viscous effects and often represents 10-20% of the turbulent boundary layer thickness, which can often be less than 1% of a total pipe diameter. The turbulent eddy motion is dampened by the wall and the velocity profile is nearly linear which means that the flow is essentially laminar. The viscous sublayer is thin and has y^+ values below 5, and it has a linear relationship between y^+ and u^+ ($u^+ = y^+$).

The buffer layer has y^+ values between 5 and 30 and is located between the viscous and the log-law sublayer. Turbulent effects are becoming more significant in the buffer layer, but the flow is still dominated by viscous effects. It is advisable to keep the first cell in a computational mesh out of the buffer layer due to difficulties modelling it accurately.

The log-law layer has y^+ values above 30, meaning that the inertial forces dominate the viscous forces. The relationship between y^+ and u^+ has a logarithmic form and can be described mathematically [3].

2.2. Heat Transfer

Thermal energy, also known as heat, can be transferred in three different ways:

- *Conduction*
- *Convection*
- *Radiation*

Conduction and convection require a temperature difference to transfer thermal energy and the energy is always transferred from a high temperature zone to a lower temperature one. Radiation is the only heat transfer mechanism that does not require a temperature difference to transfer energy.

2.2.1. Conduction

Conduction is the transfer of energy between molecules in a substance. The transfer of energy happens due to a temperature gradient between regions. Conduction can take place in a solid, a fluid or in a gas. The equation for steady one-dimensional conduction known as *Fourier's law of conduction* is shown in equation (8). The equation states that the rate of heat transfer is

proportional to the temperature difference. With κ representing the thermal conductivity of the substance, A is the area where the heat transfer takes place, ΔT is the temperature difference between two regions and Δx is the thickness of the region. The heat transfer per unit time, $\dot{Q}_{cond}$, is in Watts.

$$\dot{Q}_{cond} = -\kappa A \frac{\Delta T}{\Delta x} \tag{8}$$

2.2.2. Convection

Convection is the transfer of thermal energy between a solid surface and the adjacent fluid that is in motion. Natural or free convection is the transfer of heat energy in a fluid due to the change in density when the fluid temperature changes. An everyday example is water being heated in a kettle. The water closest to the bottom will have a temperature increase, and when the temperature rises the density decreases due to expansion of the water. The difference in density between the water layers will make the low-density water flow upwards and the higher density water at the top will sink to the bottom. The process continuously repeats itself and a natural circulation occurs.

Forced convection is when the fluid motion is forced by an external source, like a pump. The forced flow ensures a steady stream of fluid over a surface, continuously transferring heat. Steady heat transfer by convection is expressed with equation (9), which is *Newtons law of cooling*. Where A is the area for the heat transfer, T_s is the surface temperature and T_f is the fluid temperature outside the thermal boundary layer. h_c is the heat transfer coefficient for convection, which is not a fluid property, but a coefficient determined by experiments. The law states that the rate of heat loss is proportional to the difference in temperature between the object and the surroundings.

$$\dot{Q}_{conv} = h_c A(T_s - T_f) \tag{9}$$

The convective heat transfer between a Newtonian fluid and a solid surface is dependent on the fluid properties, flow velocity and the geometry of the system. The heat transfer coefficient is often expressed as a function of the Nusselt number, Reynolds number and Prandtl number as shown in the empirical equations (10) and (11) [8]. L and v represent a characteristic length and

the velocity of the fluid flow, k is the fluid conductivity and μ is the dynamic viscosity. The physical constants are usually determined through experiments for different flow geometries.

$$Nu = const \cdot Re^m \cdot Pr^n \tag{10}$$

$$\frac{h_c L}{k} = const \cdot \left(\frac{\rho v L}{\mu}\right)^m \cdot \left(\frac{c_p \mu}{k}\right)^n \tag{11}$$

The Nusselt number is the ratio between convective and conductive heat transfer, and thus represents how dominant the convection is compared to conduction. The Reynolds number covers the flow characteristics and the Prandtl number describes properties of the fluid.

2.2.3. Radiation

Heat transfer by radiation happens through electromagnetic waves due to the change in electronic configuration of atoms in a substance [9]. Thermal radiation from an object comes from the temperature of the object and is expressed by equation (12).

$$\dot{Q}_{rad} = \varepsilon \sigma A T^4 \tag{12}$$

The emissivity of the object is expressed by ε and the area and temperature are expressed by A and T, σ is the Stefan-Boltzmann constant ($5.67 \times 10^{-8}\ \frac{W}{m^2 K^4}$). The emissivity has a value between one and zero and is a measure of how much radiation is emitted compared to a blackbody which has $\varepsilon = 1$. The emissivity of an object depends on the surface, where polishing a surface will reduce the emissivity and roughening or painting the surface will increase it.

2.3. Heat Transfer in Internal Combustion Engines

The heat transfer in internal combustion engines consists of all three types of heat transfer when the heat energy is transferred from the combustion gasses through the cylinder walls to the coolant, which is shown in Figure 2. Convection is the dominant heat transfer type from the combustion gas to the cylinder wall. In diesel engines there is also a contribution from radiation in the heat transfer from the combustion gas to the wall due to radiation from soot particles.

Heat transfer through the cylinder wall happens by conduction and forced convection is present from the cylinder wall cooling surface to the coolant. Forced convection is also present in the heat transfer between combustion gasses and the cylinder head, liner, and valves. Heat is also transferred from the hot engine block to the surroundings by convection.

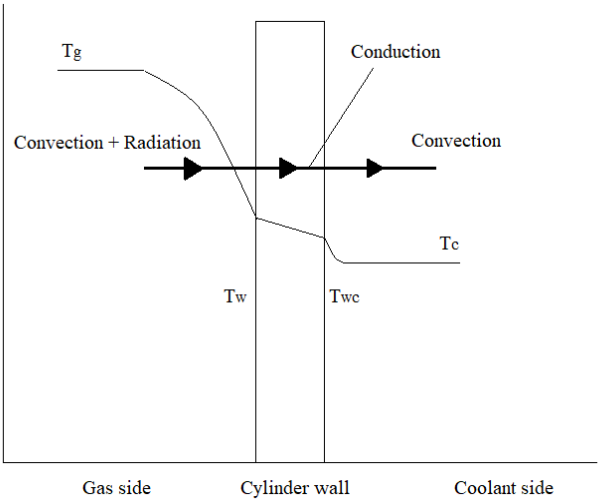

Figure 2 Heat transfer through the cylinder wall in a combustion engine [41]

The heat transfer in Figure 2 can be described as a network of three thermal resistances in series shown in equation (13). The resistances are the thermal boundary layer on the gas and coolant side, and the thermal resistance of the cylinder wall. With h being the overall heat transfer coefficient, h_g and h_c is the heat transfer coefficient for the gas and coolant side respectively. x is the thickness of the wall and k is the thermal conductivity of the wall.

$$\frac{1}{h} = \frac{1}{h_g} + \frac{x}{k} + \frac{1}{h_c} \tag{13}$$

Heat transfer plays a vital role in an engine's operation, as it affects performance, efficiency, and emissions. Higher heat transfer to the combustion chamber walls will lower the gas temperature during combustion, which will reduce the pressure and thereby the work transferred to the piston. The magnitude of heat transfer to the combustion chamber walls directly affects the efficiency of the engine.

The cooling requirement of a combustion engine depends on several factors, including engine type, speed, and load. There are several reasons for cooling an internal combustion engine.

Three of them are to ensure high volumetric efficiency, proper combustion and mechanical operation and reliability [10]. Volumetric efficiency is a measure of the effectiveness of an engine's intake process. Several factors influence the volumetric efficiency, including intake and exhaust system, valve flow friction and valve timing. The factor related to cooling is that heat transfer from the hot combustion chamber wall to the colder intake air during the intake stroke, leads to reduced volumetric efficiency. Thus, a cooler surface in the combustion chamber leads to a higher mass of air that can be trapped in the cylinder, which increases volumetric and engine efficiency [8].

Insufficient cooling can lead to overheating which can affect the mechanical reliability of the engine. Firstly, the overheating can lead to a loss of strength in the engine components. It can also lead to degradation of the lubricating oil film on the cylinder liner, which will increase friction and wear on the liner. The gas side of the cylinder liner should be kept below about 200℃ to avoid degradation of the lubricating oil film [10]. The friction losses due to the interaction between the piston and cylinder liner are increased if the lubricating oil film gets too hot and loses its properties. The friction losses are mechanical energy turned into heat due to friction, and the heat must be dissipated to the cooling system to maintain correct wall temperatures. Thermal strain is another important factor that can lead to structural failure of the engine parts. Thermal strain is proportional to the temperature gradient in the parts and thermal fatigue can occur in parts with a high cycle variation in temperature.

A typical diesel engine converts about 30-50% of the fuel energy into effective brake work, the remaining energy leaves the system as heat rejected to the atmosphere in some way. Typically, 20-35% of the energy supplied with the fuel is transferred to the coolant [10]. A small amount of the supplied energy is transferred to the environment through convection and radiation from the engine surfaces. The remaining energy leaves the system as exhaust gas enthalpy.

A simplified energy balance as shown in equation (14) and the Sankey diagram in Figure 3 provides useful information about the disposition of energy delivered with the fuel. $\dot{m}_f LHV_f$ are the fuel mass flow times the lower heating value of the fuel and represents the energy delivered with the fuel. $\dot{m}_a H_a$ is the air mass flow times the enthalpy of the intake air and combined with the fuel energy it represents the energy entering the system. The energy leaving the system is represented on the right-hand side, with P being the shaft power, $\dot{Q}_{misc}$ is

convection and radiation from the engines external surface. $H_e\ (\dot{m}_f + \dot{m}_a)$ is the energy leaving the system as exhaust gas enthalpy and $\dot{Q}_{cool}$ is the heat transfer to the coolant.

$$\dot{m}_f LHV_f + \dot{m}_a H_a = P + \dot{Q}_{cool} + \dot{Q}_{misc} + H_e(\dot{m}_f + \dot{m}_a) \qquad (14)$$

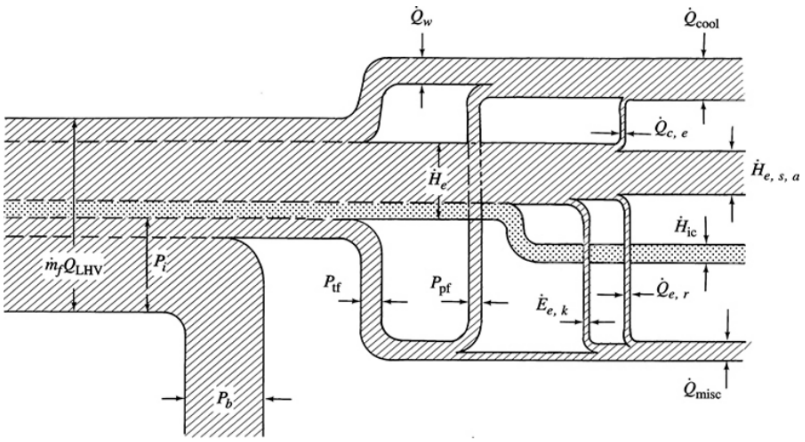

Figure 3 Typical energy flow in an internal combustion engine [8]

2.3.1. Engine Gas Side Heat Transfer

In-cylinder combustion heat transfer is complicated to model as it involves rapid changes in pressure, velocity, and temperature of the gas. Semi-empirical equations are usually used to calculate the heat transfer coefficients since many influencing factors must be determined experimentally.

The most used equation for the calculation of in-cylinder heat transfer was proposed by Woschni in 1968 [11]. Woschni's model assumes a stationary, turbulent pipe flow.
The equation is empirical and contains two convective terms, with one of them accounting for the piston motion and the other accounting for the convection due to combustion. Both terms are expressed as constants derived from experiments. They relate the fluid flow conditions during the scavenging periods and take the combustion system into consideration. The equation for the in-cylinder heat transfer coefficient h_c proposed in the original paper is shown in equation (15) [11].

$$h_c(t) = \alpha_s\, B^{-0.2}\, P(t)^{0.8}\, T(t)^{-0.55}\, v(t)^{0.8} \qquad (15)$$

α_s as a scaling factor for tuning the coefficient to a specific engine geometry. B is the bore diameter, P and T are the instantaneous cylinder pressure and gas temperature. v is an instantaneous characteristic velocity and is defined as in equation (16).

$$v = C_1 \cdot c_m + C_2 \cdot \frac{V_h \cdot T_1}{P_1 \cdot V_1} \cdot (p_z - p_0) \quad (16)$$

Where c_m is the mean piston velocity, p_z and p_0 is the average pressure with and without combustion and represents the contribution due to combustion. P_1, V_1 and T_1 are pressure, volume, and temperature at any reference condition, V_h is the cylinder swept volume. The coefficient C_1 represents the valve timing and the turbulence arising because of it. For the scavenging period a value of 6.18 is often used for C_1 and a value of 2.28 is used for the compression and expansion period. C_2 is a coefficient that describe the combustion chamber and it varies with the engine cycle. Woschni suggested using a value of 3.24 x 10^{-3} m/sec per degree crank angle for C_2. Both C_1 and C_2 are constants that must be adjusted depending on the specific engine type.

Other authors have continued the work of Woschni. Hohenberg proposed a simplified version of equation (15) in 1979 which is shown in equation (17) [12].

$$h_c(t) = \alpha_s \cdot V(t)^{-0,06} \cdot P(t)^{0,8} \cdot T(t)^{-0,4} \cdot (c_m + b)^{0,8} \quad (17)$$

The constants α_s and b were determined by comprehensive measurements of heat flux, heat balance and component temperature on various diesel engines. α_s and b was calculated by Hohenberg to be 130 and 1.4 respectively. Several studies have researched the Woschni and Hohenberg correlations, and prediction of the cycle averaged heat flux shows good agreement with experimental data. However, the instantaneous heat flux is often over- or underestimated [13].

Heat flux to the combustion chamber walls can reach very high values at top dead center during the combustion stroke. However, it can be close to zero or negative during other parts of the operating cycle. During the intake stroke there can be a negative heat flux when the cold air is heated by the hot combustion chamber walls. Figure 4 shows the heat transfer rate from the

combustion gas to the combustion chamber walls during one cycle in a four-stroke diesel engine. The figure is from the simulation that will be described in chapter 3.2.

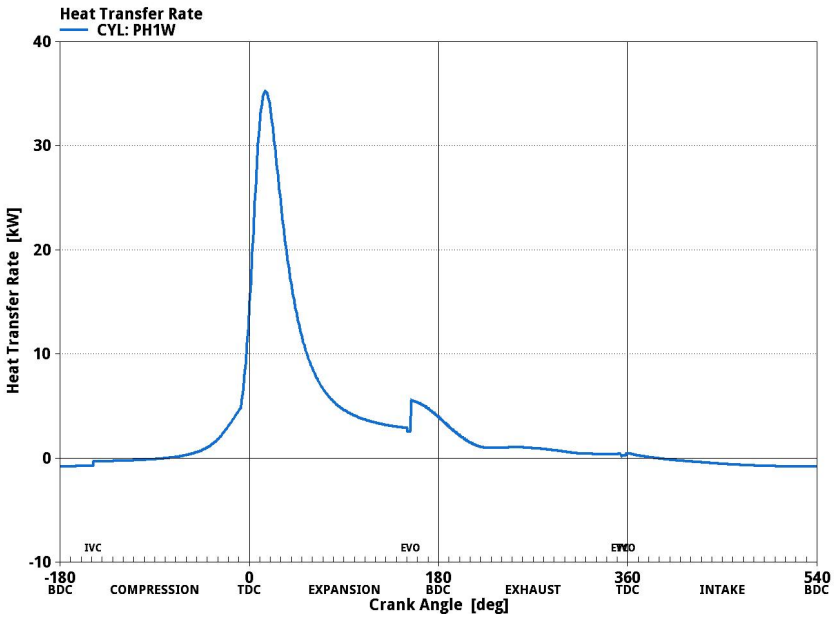

Figure 4 In-cylinder heat transfer rate for a four-stroke cycle

The heat flux into the walls changes continuously during the cycle. However, the assumption that the heat transfer process is quasi-steady is sufficient for most engineering purposes [8]. Quasi-steady in this scenario, means that the time scale for wall temperature change is much larger than the time scale for the change in gas temperature, and wall temperatures can therefore be assumed to be constant at a given load even though the gas temperature changes rapidly.

2.3.2. Engine Coolant Side Heat Transfer

Most internal combustion engines are liquid cooled with a coolant jacket surrounding the cylinder liner. There are also cooling channels in the cylinder head surrounding the valves and the exhaust ports. The cylinder liner coolant flow often consists of vertical flow with a low flow velocity, often far less than 1 m/s. Flow velocities below 0.5 m/s leads to an increased influence of free convection compared to forced convection. A water and ethylene-glycol mixture are usually used for cooling purposes in internal combustion engines. Where water is an effective coolant with many desired properties including high specific heat capacity, high enthalpy of vaporization and high thermal conductivity. One drawback with water is the freezing temperature of 0 °C at atmospheric pressure, which makes it unsuitable for use in colder regions.

An anti-freeze agent (e.g., glycol) is therefore added to lower the freezing temperature. There are also other additives in the coolant that protects against corrosion and foaming. The mixture of water and glycol degrades the thermophysical properties of the coolant when compared to water by itself [8].

The heat transfer coefficient for the coolant side can be a challenge to determine in combustion engines. Information about the coolant flow velocity, density, specific heat capacity and thermal conductivity must be known. Other factors are the thermal load and flow conditions at the specific locations and the rough surface on the coolant side of the cylinder liner should also be accounted for. Therefore, there can be many different heat transfer coefficients throughout the engines cooling system [14].

A variety of correlations have been developed to determine the heat transfer coefficient in forced convective flows. For fully developed turbulent flow in a smooth circular pipe the Nusselt number (Nu) can be estimated with the Dittus-Boelter correlation in equation (18), which is valid for flows with Re > 2500 and Prandtl number between 0.7 and 120 [15].

$$Nu = 0.023 Re^{0,8} Pr^{0,4} \tag{18}$$

Empirical values for the heat transfer coefficient are often relied upon in simple problems. Some typical guide values for the coolant side heat transfer coefficient are [14]:

Free convection:	400 - 2 000 W/m^{2}K
Forced convection:	1 000 - 4 000 W/m^{2}K
Nucleate boiling:	2 000 - 10 000 W/m^{2}K

Coolant boiling can occur in high temperature regions, and it is an important heat transfer mechanism in liquid cooled engines. The high heat transfer coefficient when boiling occurs restricts the increase in temperature of the metal. Nucleate boiling can occur at local hot spots in the cooling system. Nucleate boiling is when vapor bubbles are nucleated and grow from separate sites and liquid remains in contact with part of the heated surface. This phenomenon increases the movement of the liquid and thereby the heat transfer. At higher thermal loads above the critical heat flux, the vapor bubbles will merge into a more continuous vapor film, which will have an insulating effect and deteriorate the heat transfer (transition boiling) [14].

If the heat transfer is assumed to be a combination of both convection and nucleate boiling, then the heat flux q is given by equation (19) [10]. The convective and boiling heat transfer coefficient is represented by h_c and h_b respectively. T_w is the wall temperature, T_1 is the liquid bulk temperature and T_s is the saturation temperature of the coolant.

$$q = h_c(T_w - T_1) + h_b(T_w - T_s) \tag{19}$$

2.4. Nanofluid

Heat transfer is present in a vast variety of industrial applications, including electrical devices, mechanical equipment, and engines. Thermal management in these systems is crucial with regards to reliability and operability. For a lot of industrial equipment there is a focus on reducing size and weight, while also increasing power density. This often leads to increased heat flux that must be dissipated to the environment. The amount of maximum heat dissipation is often a limiting factor for technological advancements.

One method to increase heat transfer is to increase the surface area of the thermal contacts. However, this can lead to an increase in size and weight of the system, which is often undesirable. Other methods are to roughen the surface or increase the flow velocity over the surface. All three methods can result in increased system pressure and greater pumping power. There is a limit to how much heat transfer can be improved by these measures. To further increase the heat transfer it is possible to change the thermodynamic properties of the coolant or change coolant entirely. Dispersing high conductivity nanosized particles in a base liquid can result in higher thermal conductivity, but it comes with several challenges. Settlement of particles, abrasion and increased viscosity can make the solution unattractive.

Development of nanotechnology has resulted in several methods to produce nanoparticles of different materials, ranging from 10 to 500 nm in size. The improved thermal conductivity of nanofluids can lead to increased heat transfer rate even at low volume fractions. The size of nanoparticles is relatively close to the size of molecules of the base fluid, and thus they can form stable suspensions with little settling over longer periods of time. Nanoparticles are often made of materials like alumina, silica, and copper oxide. Metals such as copper and gold are

also used. The particles are suspended in a base fluid which is often water or an organic fluid like ethanol or ethylene glycol. The volumetric concentration of particles in the base fluid is usually below 5% [16].

Nanofluids as a heat transfer medium gained interest after several reports documented an increase in thermal conductivity in nanofluids compared to the base fluids [17]. One study reported a 40% increase in thermal conductivity by using 0.3 vol% copper nanoparticles with a diameter of 10 nm in ethylene-glycol base fluid [18]. Another study reported an increase in thermal conductivity of 10-25% with 1-4 vol% alumina nanoparticles in water [19]. However, the thermal conductivity may not be the only property influencing the heat transfer coefficient. Other studies have proposed dispersion models to explain the increase in convective heat transfer in nanofluids. This approach assumes that the heat transfer enhancement comes from two factors. The first is higher thermal conductivity and the second is the dispersion of nanoparticles [20].

Increase in heat transfer with nanofluids is not only dependent on thermal conductivity but also the viscosity of the fluid, where an increase in viscosity will negatively affect the heat transfer coefficient in turbulent flows. The effect of viscosity in laminar flows does not seem to change the heat transfer coefficient. A general observation with nanofluids is that the viscosity increases with decreasing particle size and the thermal conductivity increases with increasing particle size. Adding nanoparticles to a base fluid will change both the thermal conductivity and the viscosity of the fluid. And if the increase in thermal conductivity of the heat transfer fluid is significantly less than the increase in viscosity, it could result in a lower heat transfer coefficient compared to the base fluid [21] [22].

A study from 2018 critically assessed the validity of the assumption that empirical correlations for calculating the convective heat transfer coefficient, equation (11), is applicable for stable homogeneous nanofluids when the thermodynamic properties of the nanofluid are used [23]. The study concluded that “Newtonian nanofluid flow is sufficiently described employing Nusselt number correlations obtained for single-phase heat transfer liquids such as water when thermophysical properties of nanofluid are utilized”. This assumes that the heat transfer enhancement comes only from the improved thermophysical properties of nanofluids. The study also concluded that the increased heat transfer of nanofluids was proportional to the increase in thermal conductivity compared to the base fluid.

Guidelines for evaluating nanofluid heat transfer performance are given in the 2018 study with the following steps [23]:

- Evaluate if the nanofluid shows Newtonian behavior or not. The following method is only applicable for Newtonian fluids.
- Measure the thermal conductivity and viscosity of the nanofluid in the temperature interval of interest.
- Calculate density and heat capacity using equation (20) and (21). Where ϕ represent the particle concentration and nf, np and bf is the nanofluid, nanoparticle and base fluid property.

$$\rho_{nf} = \phi\rho_{np} + (1-\phi)\rho_{bf} \tag{20}$$

$$c_{p,nf}\rho_{nf} = \phi c_{p,np}\rho_{np} + (1-\phi)c_{p,bf}\rho_{bf} \tag{21}$$

- Use these thermophysical properties with traditional correlations for convective heat transfer of single-phase liquids.

Another aspect of nanofluid heat transfer is the effect from Brownian motion, which is the random movement of particles suspended in a fluid. The random motion increases collisions between the fluid molecules and the nanoparticles and can lead to enhanced thermal conductivity. Brownian motion is possibly one of the main reasons for the enhancement of thermal conductivity in nanofluids [24] and this has led to development of new models that are dependent on temperature for evaluation of thermal conductivity [25]. One study incorporated the effects of Brownian motion in a natural convection heat transfer model for nanofluids. The study concluded that Brownian motion enhanced the heat transfer at any volume fraction of nanoparticles. And by neglecting the effect of Brownian motion the heat transfer was deteriorated [26].

3. Methodology

An often-used method for prediction of an engines thermal field is to use a 3D combustion simulation to determine the spatial temperature distribution in the combustion chamber. The boundary conditions are then used in a detailed CFD analysis to predict the thermal field of the engine.

One study from 2011 used a heat source obtained from 1D and 3D combustion simulation in a conjugate heat transfer simulation. The cycle-averaged heat source was applied to the surfaces of the combustion chamber. The study concluded that the conjugate heat transfer analysis generated a temperature field which correlated well with experimental test results. The comparison was made based on coolant temperature rise, pressure drop, and point measurements of temperature at selected locations in the cylinder head [27]. Similar methodologies are described in several papers [2] [28] [29].

The objectives of this thesis are focused on the coolant side heat transfer and the relative difference between coolants. Due to the time restriction of the project and the availability of software licenses, a 3D combustion model was not developed. Instead, a 1D engine simulation is used to predict the thermal boundary condition for the CFD simulation. Though not as accurate as 3D combustion modeling, it is sufficient to determine a relative difference between different coolants.

The following sub-chapters will describe how the work was carried out and how the CFD model was created. The structure of the chapter is listed below:

- General information about the research engine
- Presentation of the 3D engine model
- Calculation of coolant side heat transfer coefficient in STAR CCM+
- Calculation of heat transfer to coolant in Realis WAVE
- Boundary conditions for the CFD model
- CFD model mesh
- Explanation of physics models used in the CFD model.

3.1. The Diesel Engine

The engine used for this work is a Petter PH1W single-cylinder diesel engine [30]. It is a four-stroke, water-cooled engine with a rated power output of 6.4 kW at 2000 rpm. The specific engine is installed in the engine laboratory at Western Norway University of Applied Science. The engine is used as a research engine and is well instrumented. A short summary of the main engine data is listed in Table 1.

Table 1 Petter PH1W engine data

No. of cylinders	1
Engine type	Four-stroke
Bore	87.3 mm
Stroke	100 mm
Displacement	0.659 liter
Compression ratio	16.5: 1
Power at 2000 rpm	6.4 kW
Power at 1500 rpm	4.7 kW

3.2. In-Cylinder Heat Transfer Boundary Condition

A boundary condition for the CFD simulation of the coolant is the heat rejected from the combustion gas to the combustion chamber walls. To determine the amount of heat rejection a 1D model of the engine was created in the software Realis WAVE, which is a 1D gas dynamics and engine simulation software. It can be used to analyze the dynamics of pressure waves, mass flows and energy losses of various systems.

The 1D model is a further development of the model used for the same engine in a previous master thesis by K. Skaar in 2016 [31]. The existing model was not properly set up for calculation of heat transfer and parameters were updated with knowledge gained from the 3D model of the engine. The 3D model of the engine made it possible to extract the coolant surface areas inside the engine and to determine the volume of solid material. Both parameters are important to determine the heat transfer to the coolant.

The engine was disassembled for most of this thesis work due to maintenance and rebuilding of the cooling system. This will make the engine more suitable for experimental heat transfer studies. Therefore, some of the inputs for the 1D engine model is based on empirical data obtained from a 2017 master thesis by J. Tingstad, which was also done on the same engine [32]. The thesis work consisted of converting the fuel injection system on the diesel engine to common rail injection. Several tests with detailed measurements were published, and a test done at 1500 rpm at different torques shown in Attachment 1 serves as the basis for this 1D engine model. The engine had issues with vibration at higher speeds than 1500 rpm, thus there is no test data for 2000 rpm and maximum power. Some of the data from the 1500 rpm test was used as input for the 1D model, and other data was used to validate the simulation results with the physical engine.

3.2.1. Coolant Side Heat Transfer Coefficient

The only input parameter for the 1D model which was not attained from the experimental data and engine manual, was the heat transfer coefficient between the coolant and the coolant walls. There are two options for the coefficient in WAVE. The first option is to use the correlation setting, which is an empirical equation where WAVE calculates the coolant heat transfer coefficient. According to the WAVE manual, correlation should only be used when the cooling water is hot, the engine is warm and when nucleate boiling is expected. The empirical equation is shown in equation (22) [33], where h is the coolant heat transfer coefficient and Q is the heat flux in W/m^2.

$$h_{coolant} = 1.48 \cdot Q^{0,644} \tag{22}$$

The other option is to enter a user specified value. The CFD model which will be described later in chapter 3.3 was used to calculate the coolant heat transfer coefficient. The fluid used for the reference simulation and calculation of the heat transfer coefficient was pure water. A heat source was applied to the cylinder liner and head, and a heat transfer coefficient was then calculated by the following method.

The heat rejected to the coolant was determined by equation (23), where $\dot{m}$ is the coolant mass flow, C_p is the specific heat capacity of the coolant, and the temperature difference between inlet and outlet is represented by $(T_{out} - T_{in})$.

$$\dot{Q} = \dot{m} \cdot C_p \cdot (T_{out} - T_{in}) \tag{23}$$

The heat rejected to the coolant can also be determined by equation (24). For the liner, $A_{coolant}$ is the coolant side liner surface area, $\bar{T}_{wall}$ is the average surface temperature on the coolant side and $\bar{T}_{fluid}$ is the average fluid bulk temperature. h_c is the unknown heat transfer coefficient.

$$\dot{Q} = h_c \cdot A_{coolant} \cdot (\bar{T}_{wall} - \bar{T}_{fluid}) \tag{24}$$

By combining equation (23) and (24) we get an expression for the heat transfer coefficient shown in equation (25).

$$h_c = \frac{\dot{m} \cdot C_p \cdot (T_{out} - T_{in})}{A_{coolant} \cdot (\bar{T}_{wall} - \bar{T}_{fluid})} \tag{25}$$

The heat transfer coefficient was calculated for the cylinder liner and head surface separately. The magnitude of the applied heat source to the liner and head surface was varied between 500 and 2500 Watts and the resulting coolant heat transfer coefficient remained stable. However, the difference was seen in the wall temperatures, as an increased heat source resulted in higher wall temperatures. The results from the correlation and CFD calculation are shown in Table 2. The magnitude of the heat transfer coefficient does not vary much between the two calculation methods which may indicate that the assumptions for using the correlation setting are valid in this scenario.

Table 2 Coolant side heat transfer coefficient

	CFD calculation	**WAVE Correlation**
Liner heat transfer coefficient [W/m^2 K]	1518	1485
Head heat transfer coefficient [W/m^2 K]	1433	1253

3.2.2. 1D Engine Model

When simulating engine processes, the governing equations must be solved on a step-by-step basis, often with increments of 1-degree crank angle. The first law of thermodynamics is used as a basis for calculating the internal combustion engine processes. The differential form of the first law of thermodynamics for an open thermodynamic system is shown in equation (26). The equation states that the change in internal energy (U) is equal to the change in energy (Q) supplied to the system, subtracting the work (w) done by the system plus the sum of enthalpy (H) change.

$$\frac{dU}{dt} = \frac{dQ}{dt} - \frac{dw}{dt} + \sum \frac{dH}{dt} \tag{26}$$

The combustion process for diesel engines is usually modelled as a single zone. Whereas for spark ignited engines a two-zone model is often used, dividing the combustion chamber into a burned and unburned zone. For a diesel engine single-zone combustion model and with the assumption that the gas behaves as a perfect gas, equation (26) turns into the energy balance shown in equation (27) [10]. The left side of the equation describes the change in internal energy (u) as a function of temperature and crank angle (θ). The right side describes the displacement work from the piston, the heat flows (Q) and the stagnation enthalpy (H) of any flows entering or exiting the control volume.

$$m\frac{\partial u}{\partial t}\frac{dT}{dt} + m\frac{\partial u}{\partial \theta}\frac{d\theta}{dt} = -\frac{mRT}{V}\frac{dV}{dt} + \sum \frac{dQ}{dt} + \sum H\frac{dm}{dt} \tag{27}$$

Work (w) from the piston is calculated from the pressure (p) and volume (V) change in the cylinder as shown in equation (28).

$$\frac{dw}{dt} = -p\frac{dV}{dt} \quad with \quad p = \frac{mRT}{V} \tag{28}$$

To describe the change in temperature and internal energy a combustion model is needed. The primary goal of a combustion model is to calculate the heat release rate from combustion. In a diesel engine, which is a compression ignited engine, the combustion is influenced by several factors including: ignition delay, the amount of pre-mixed and diffusion combustion. All of

which are complex to describe. The combustion models in WAVE uses equilibrium chemistry to convert the fuel and air into combustion products during combustion and calculates the amount of air and fuel that has reacted at each timestep with an empirical relation [5]. Several models are available in WAVE and the diesel Wiebe combustion model was the most suitable one for the Petter diesel engine as it is the primary combustion sub-model for diesel engines in WAVE. The resulting heat release rate is shown in Figure 5 with start of injection at 26° BTDC and start of combustion at 9° BTDC.

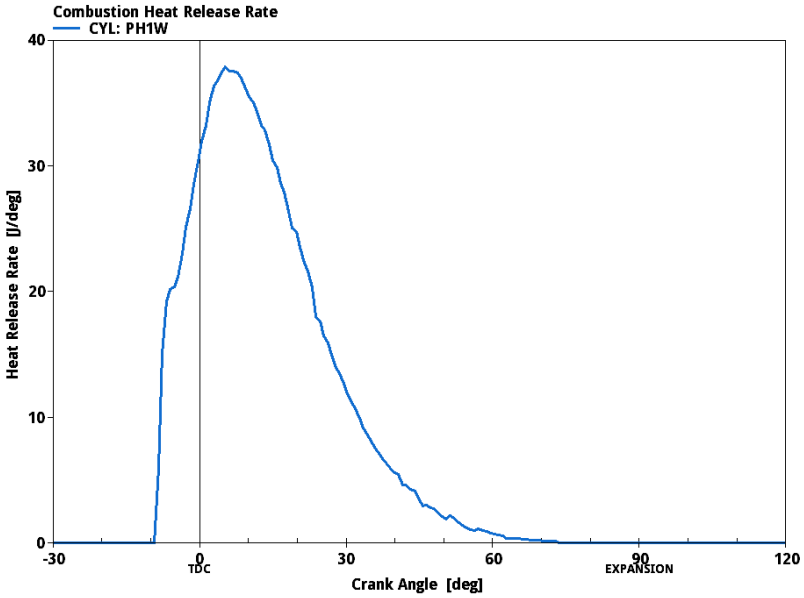

Figure 5 Combustion Heat Release Rate 1D Engine Model

The heat transfer from the combustion gas to the combustion chamber walls is modelled by the Woschni equation described in chapter 2.3.1.

Results from the energy balance are in terms of indicated performance and does not account for the frictional losses in the engine. To get the brake performance, frictional losses must be predicted. The Chen-Flynn correlation for the frictional losses from 1965 is often used and is shown in equation (29) [34]. Unlike other correlations Chen-Flynn accounts for the pressure loading from combustion. P_{max} is the maximum pressure during combustion and c_m is the mean piston speed. $fmep$ is the frictional mean effective pressure and represents the frictional losses.

$$fmep = 0{,}137 + \frac{P_{max}}{200} + 0{,}162\, c_m \tag{29}$$

Heat transfer in the engine is handled by the heat transfer sub-model in WAVE which represent the combustion chamber as a simplified thermal resistance network as illustrated in Figure 6. The cylinder head and liner are modeled as a one-dimensional thermal resistance. Meaning that the heat is transferred from the combustion gas via the gas side cylinder wall, through the solid material, to the coolant side surface and then to the coolant itself. There is also a thermal resistance link between the cylinder head and the valves, where the contact resistance is exerted on the valve seats when the valves are closed. The piston is modelled as a Y-junction, which means that heat is transferred from the combustion gas to the piston structure and then diverted into two directions. One part of the heat goes to the piston oil cooling and the other part goes to the piston skirt. The heat transfer between the piston and liner is a contact thermal resistance due to the contact between the piston rings and the liner. The cylinder head and liner are thermally isolated from each other due to the thermal resistance of a head gasket.

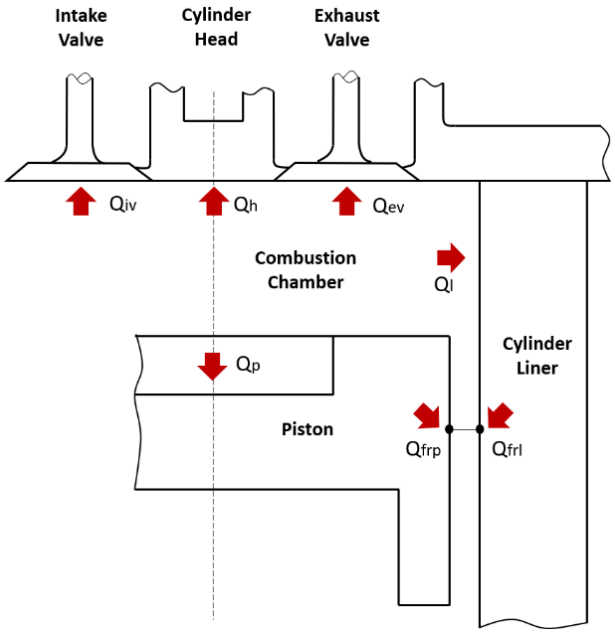

Figure 6 Heat transfer sub-model in WAVE

All the input data used for the 1D engine model, such as valve and injection timing are listed in Attachment 3 and includes the calculated coolant heat transfer coefficients from the CFD calculation. Figure 7 shows the visualization of the 1D engine model, with a PID-controller that regulates the fuel mass flow needed for an engine torque of 30 Nm at 1500 rpm.

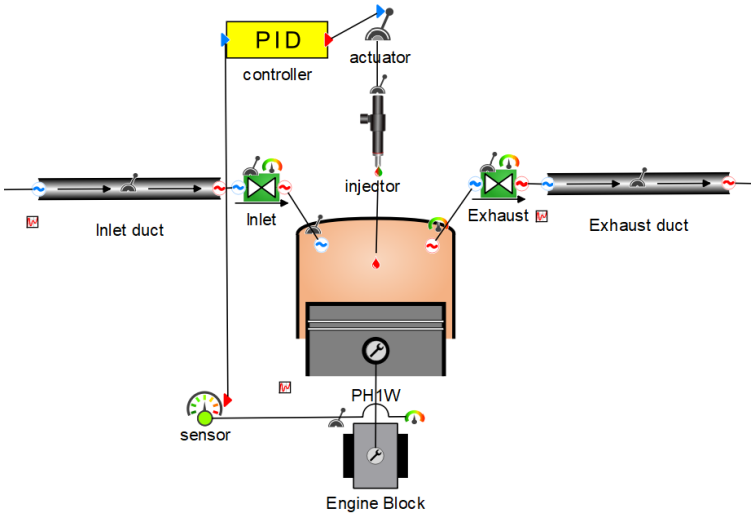

Figure 7 1D model of the Petter Diesel engine in WAVE

To determine the validity of the 1D model a comparison was made between the experimental data, which the model is based on, and some of the outputs from the simulation. The 1D model predicts the engine parameters with reasonable accuracy as shown in Table 3. The brake thermal efficiency for the 1D model is 0.6 percent point higher than the experimental data and the exhaust temperature is only off by 1.5 %. Other outputs are more inaccurate, but the model still seems suitable for the purpose of comparing different coolants.

Table 3 Validation of the 1D-simulation model

	1D Model Outputs	**Experimental Data** [32]
Exhaust temperature [°C]	531	523
Brake thermal efficiency [%]	32.6	32
Fuel consumption [kg/h]	1.22	1.37
IMEP [bar]	7.94	7.12
Pmax [bar]	71.52	75.70

The results from the 1D model that are needed as boundary conditions for the CFD analysis are the coolant side head and liner heat transfer which are listed in Table 4. The coolant side head and liner heat transfer are the cycle averaged magnitude of heat energy transferred to the coolant from the combustion chamber through the cylinder head and liner. Both values will be used as boundary conditions in the CFD model. The coolant side liner heat transfer consists of all the thermal loads acting on the cylinder liner. This includes the heat fluxes due to combustion, friction from piston rings and skirt, and the conduction from the piston.

Table 4 1D engine model heat transfer results

Head coolant side heat transfer	1069 W
Liner coolant side heat transfer	2330 W

3.3. CFD Simulation Setup

The software used for the CFD simulation is Simcenter STAR-CCM+ v.2020.1 which ran on a computer with a 12 core AMD Ryzen 9 5900X CPU combined with 16 GB of RAM. This sub-chapter will describe the process of creating the complete CFD model.

3.3.1. 3D Engine Model

To create a 3D model that resembles the engine as close as possible the engine had to be disassembled so that all parts could be measured and studied. Attempts was made to get the measurements of the engine parts with a 3D laser scanner, but this proved to be unsuccessful. All measurements of the engine were therefore taken with different sized Vernier calipers, and the measuring method could result in some deviations between the 3D model and the real engine. The cooling channels in the cylinder head were especially challenging to model due to it being a closed space with poor accessibility. A computer aided design (CAD) software CREO Parametric was used to create the engine model. The final 3D model is made of five parts, the cylinder block, cylinder liner and the cylinder head with two valves. Figure 8 shows the dismantled cylinder block and head on the left and the assembled model on the right. The box dimensions of the assembled engine are 211 x 156 x 269 mm (L x W x H).

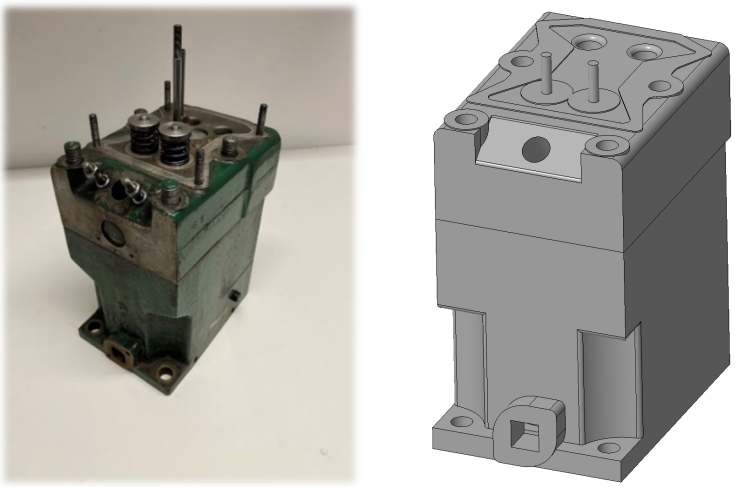

Figure 8 Dismantled engine and the 3D model.

Figure 9 shows the rear and cross-section of the engine model. The coolant inlet has a quadratic shape and is located at the bottom of the cylinder block. The coolant enters at the bottom of the liner and travels vertically up to the cylinder head through four passages. The coolant outlet is located at the center of the cylinder head, between the exhaust and air inlet ports.

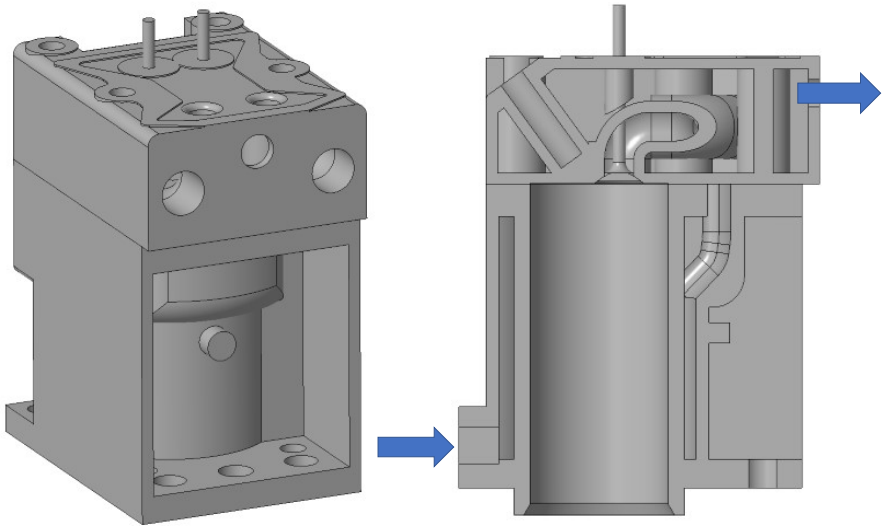

Figure 9 3D engine model, rear and cross-section view

3.3.2. Mesh

The process geometry is transformed to a computational region and is discretized into a finite number of cells that make up the computational mesh. A shared boundary between two regions can be joined by an interface that can allow thermal energy to flow between the two regions. Star CCM+ uses the finite volume method (FVM) to discretize the computational domain. The method divides the domain into finite volumes and discretizes the differential governing equations so they can be applied to the grid of volumes.

The computational domain of the engine is divided into a solid and fluid region as shown in Figure 10. The regions were meshed separately, with a finer mesh for the fluid region. The solid region was discretized by polyhedral cells, and the fluid region was discretized using polyhedral cells with a multi-layer prismatic mesh adjacent to the walls to correctly capture the turbulent boundary layer and local temperature gradients. The mesh at the coolant outlet was extended to prevent reverse flow conditions at the outlet.

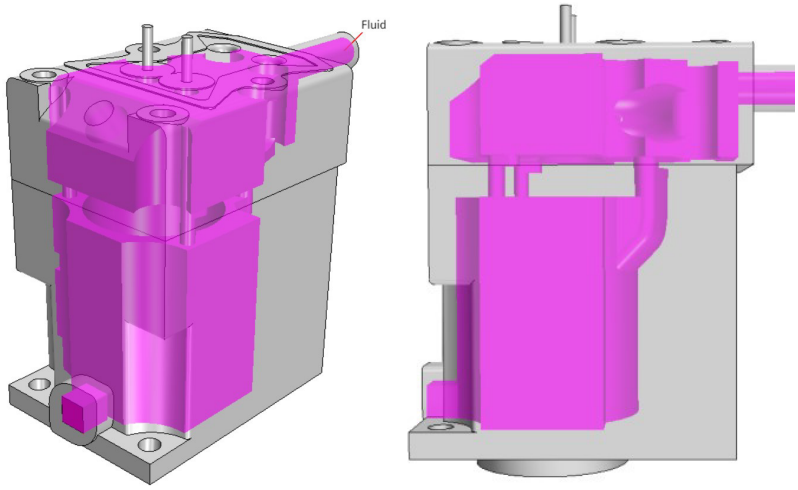

Figure 10 Solid and fluid region

To determine the required cell size in the computational domain a mesh independence study was performed. Seven different meshes were tested, ranging from a combined fluid and solid region cell count of 0.6 million cells for the coarsest mesh up to 23.8 million cells for the finest. The target cell size was reduced by 50% for each iteration (e.g., 80, 40, 20, 10, 5), the other mesh parameters were kept the same. To determine when convergence was reached several parameters were examined, including wall and fluid temperatures. The graph in Figure 11 shows how the computation time changes as the cell count increases. At the same time, the average surface temperature on the coolant side of the cylinder liner decreases until it converges at about 101°C. Based on Figure 11 a total cell count between 7.6 and 13.8 million cells seems to give the best tradeoff between computational time and accuracy.

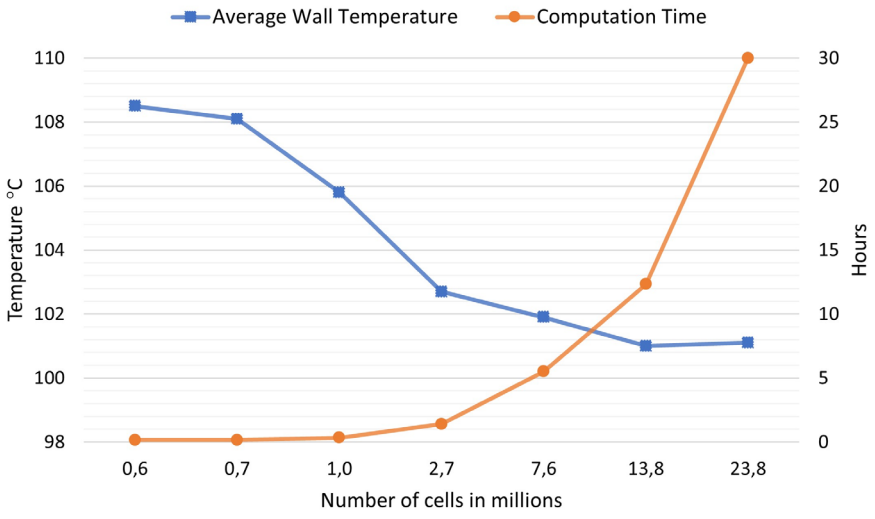

Figure 11 Mesh independence study

However, the residuals for the governing equations did not converge as well for the finer meshes that had more than two million cells, meaning that the accuracy of the simulation can be questioned. A mesh with a total cell count between one and two million achieved the best convergence of residual values and was therefore used instead of the finer mesh.

The final mesh for the fluid region uses the values listed in Table 5 and the surface mesh can be seen in Figure 12. The target surface size for the cells was set to 2 mm, which was also used in a similar study that explained a complete CFD/CHT methodology for combustion engines [28]. The only difference between the mesh used for water and the mesh used for nanofluid is the height of the first prism cell layer adjacent to the wall, which is changed to maintain y^+ values close to 1 due to the higher viscosity of nanofluids.

Table 5 Fluid mesh parameters

Cell count	602 124
Target surface size	2 mm
Minimum surface size	0.06 mm
Number of prism layers	3
Prism layer stretching	1.2
Prism layer total thickness	0.5 mm

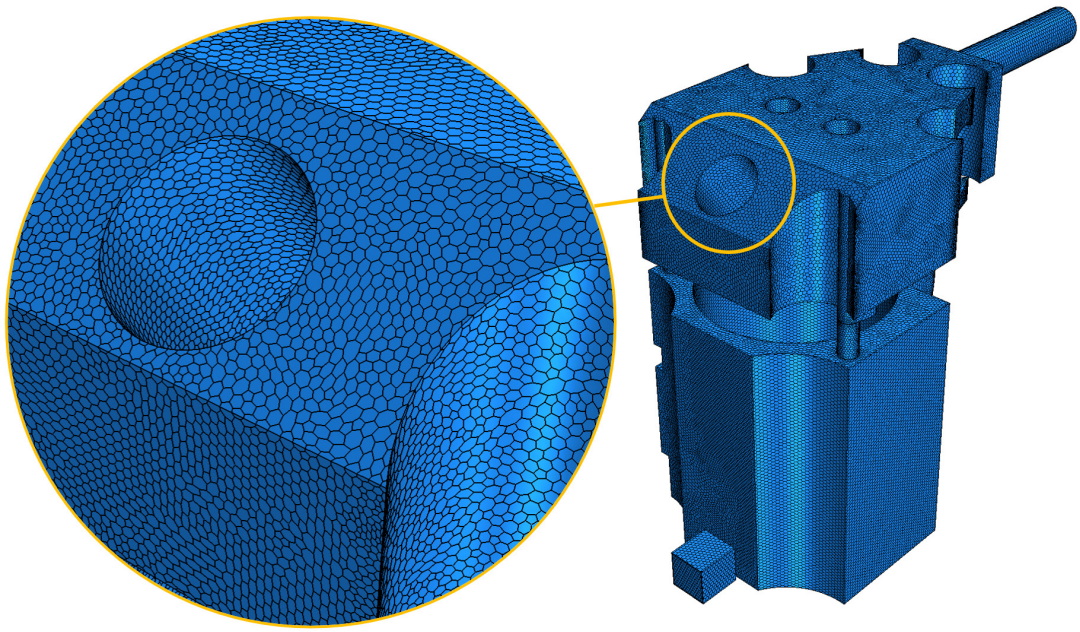

Figure 12 Fluid surface mesh

The solid mesh is coarser than the fluid mesh with a target cell size that is 1.6 times higher. A finer mesh was tested on the solid region, which only affected computational time and not the results. The main parameters for the solid mesh are shown in Table 6. The combined cell count for the fluid and solid mesh is about 1.2 million.

Table 6 Solid mesh parameters

Cell count	599 208
Target surface size	3.2 mm
Minimum surface size	0.6 mm

A cross-section of the solid and fluid mesh can be seen in Figure 13, with the layers of prismatic cells in the cylinder liner coolant jacket shown in the zoomed view.

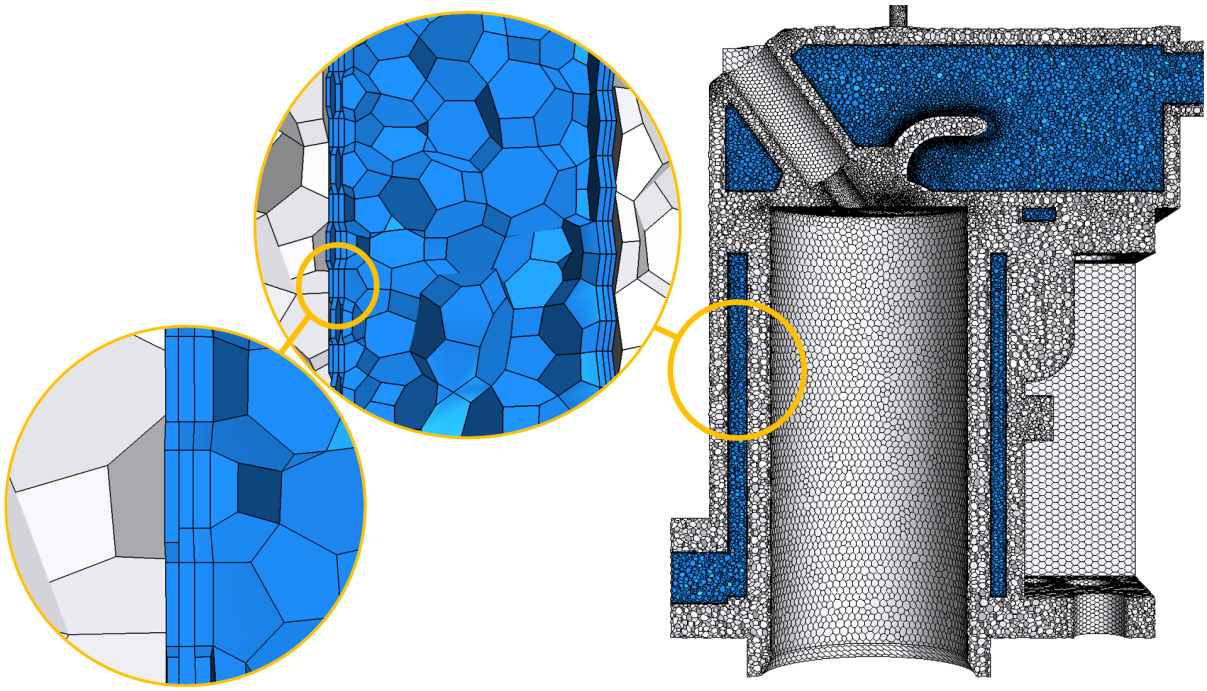

Figure 13 Solid and fluid mesh

Poor quality of the volume mesh can reduce the accuracy of the obtained solution. Several cell metrics are available to determine if the quality is acceptable, including mesh density, y^+, skewness angle and cell quality. A cell quality of 1.0 is considered a perfect cell and one example of such a cell is a cube. Cells with a quality less than 1.0e-5 are considered bad. The bar chart in Figure 14 shows the cell quality for the fluid and solid mesh. The overall cell quality of the mesh is acceptable and should not cause invalid solutions. The skewness angle of the

cells was also acceptable, where most cells had a skewness angle between 10° and 50°, which is good considering that a skewness angle greater than 85° is considered bad.

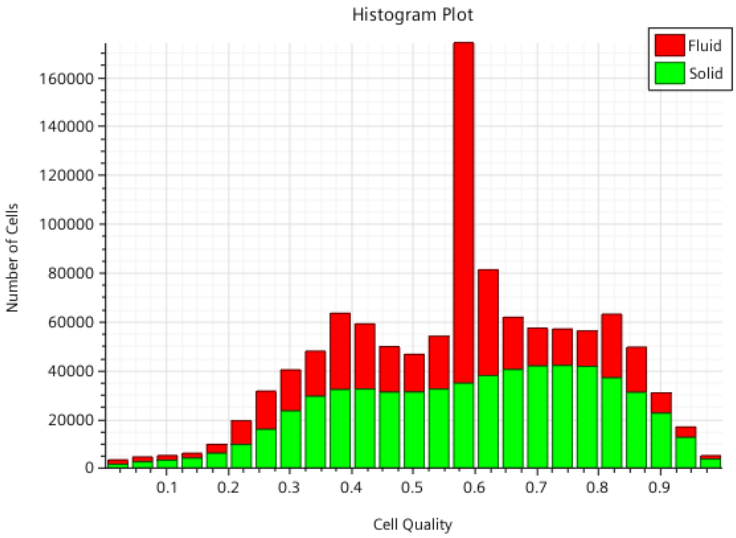

Figure 14 Cell quality bar chart

3.3.3. Coolant Properties

The type of coolant most often used in combustion engines is a mix of water and ethylene glycol which gives the coolant antifreeze properties. The engine used for this work has been running with water as coolant and water was used during the experimental tests that the 1D engine model is based on [32]. Water is therefore also used in the reference simulation. The coolant properties for the reference simulation are based on water at 75 °C and are listed in Table 7.

Table 7 Reference simulation fluid properties [3]

Coolant type	Water
Temperature	75 °C
Specific Heat Capacity c_p	4193 J/kg·K
Conductivity k	0.667 W/m·K
Density ρ	974.7 kg/m^3
Dynamic Viscosity μ	0.378 mPa·s
Prandtl number Pr	2.38

The nanofluid properties are taken from a master thesis by S. Ruud [35], where the work consisted of preparation and characterization of nanofluid properties using 50 nm carbon black nanoparticles, PVP-surfactant, and water as base fluid. Thermophysical properties for several carbon black nanofluid concentrations are presented in the thesis. Table 8 shows the properties

for the two nanofluids that are being used for the simulations. One fluid contains 2.5 weight percent carbon black nanoparticles and the other contains 10 weight percent. The increased concentration of nanoparticles results in higher fluid conductivity, but at the expense of increased viscosity.

Table 8 Nanofluid simulation fluid properties

	2.5 wt% CB	**Relative to water**
Temperature	75 °C	
Specific Heat Capacity c_p	4113 J/kg·K	0.98
Conductivity k	0.6892 W/m·K	1.033
Density ρ	986.4 kg/m^3	1.012
Dynamic Viscosity μ	0.4567 mPa·s	1.208
	10 wt% CB	**Relative to water**
Temperature	75 °C	
Specific Heat Capacity c_p	3876 J/kg·K	0.924
Conductivity k	0.768 W/m·K	1.151
Density ρ	1019.8 kg/m^3	1.046
Dynamic Viscosity μ	0.9457 mPa·s	2.5

3.3.4. Boundary Conditions

The coolant flow rate of the cooling system was measured before the engine was disassembled. The result was a coolant flow rate of 8 l/min, which translates to a flow velocity of 0.252 m/s at the quadratic coolant inlet. The pressure at the coolant outlet is set to atmospheric pressure because the coolant outlet flow goes to an open tank.

Boundaries facing the combustion chamber (i.e., cylinder head and liner gas side) have a heat source applied to them where the magnitude of the heat source comes from the 1D engine simulation presented in chapter 3.2.2. The boundary condition heat fluxes used for the simulation are not cycle-resolved due to the thermal inertia of the solid region. Cycle-averaged values are thus used. The heat sources are applied uniformly on the liner and head surface as shown in Figure 15. The exhaust and inlet valves are fixed in closed position with a thermal contact between the valve and the valve seat.

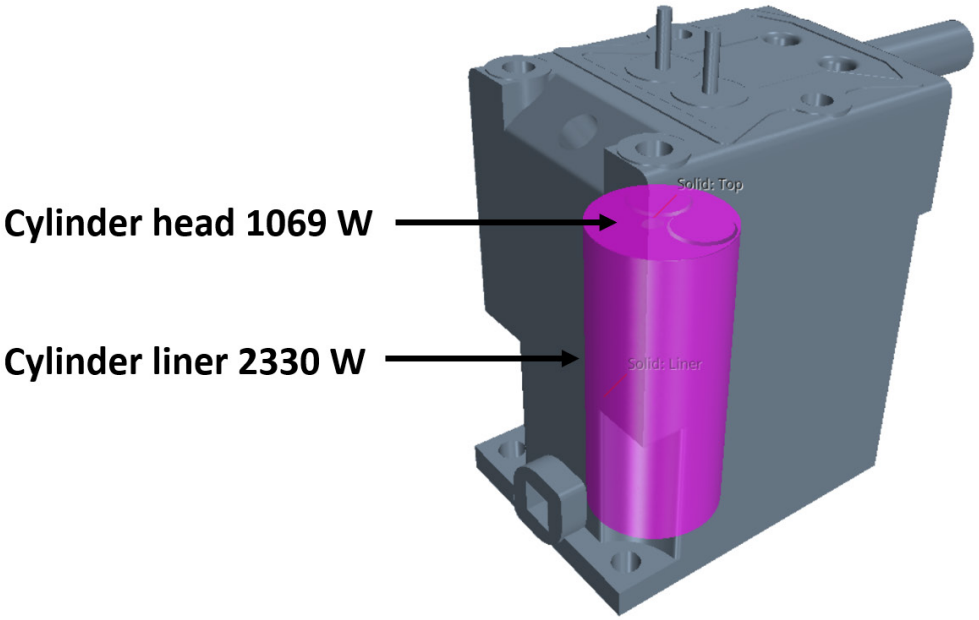

Figure 15 Heat source boundaries

Heat transfer from the hot surfaces due to radiation is calculated by equation (30) [9], where ε is the emissivity, σ is the Stefan-Boltzmann constant and A is the engine surface area exposed to ambient air. The surface temperature of the engine and ambient temperature is represented by $(T_{sur}^4 - T_\infty^4)$. An emissivity factor of 0.9 is used for the engine surface, which is the emissivity factor for the green paint that covers the engine surfaces [36].

$$\dot{Q} = \varepsilon\sigma A\,(T_{sur}^4 - T_\infty^4) \tag{30}$$

Convective heat transfer from the hot surfaces of the engine to the environment is handled by assigning a convective boundary condition to the surfaces exposed to the ambient air. Calculation of the heat transfer coefficient is quite cumbersome and is hence shown in Attachment 4. The result from the calculation is a heat transfer coefficient of 6.6 W/m^{2}K.

3.3.5. Physics

Nanofluids can be modelled with both single- and two-phase models. A study from 2015 compared the predictions of five types of CFD models to model turbulent forced convection of Cu-water nanofluid [24]. The study included two single-phase models and three two-phase models. The results were compared with experimental investigations from literature. The study

recommended to use the Newtonian single-phase or Eulerian-Lagrangian two-phase model. The study mentioned in chapter 2.4 [23] also concluded that Newtonian nanofluid flow is sufficiently described employing Nusselt number correlations obtained for single-phase heat transfer liquids such as water when thermophysical properties of nanofluid are utilized. Given this information, it was decided to model the nanofluid as a single-phase liquid and use the Newtonian single-phase model for the nanofluid simulations.

The coolant flow rate in the current engine setup is rather low at 8 l/min. To determine whether the coolant flow is laminar or turbulent, several cross-sections of the flow were examined. The average flow velocity at the coolant inlet results in a Reynolds number of 14 500, indicating turbulent flow in that region. Other regions, like the flow surrounding the cylinder liner which is visualized in Figure 16, has a Reynolds number of about 2000 using the coolant properties from Table 7 and the average velocity in the area of 0.0252 m/s. However, as the figure illustrates, the flow velocity varies a lot over the cross-section, with velocity magnitudes ranging from 0 to 0.19 m/s. Thus, it is likely that there is a mix of laminar, transitional, and turbulent flow regimes in the cross-section. Due to the geometry and rough surface of the cooling channels, which also contributes to turbulent flow [37], a low Reynolds number turbulence model is used.

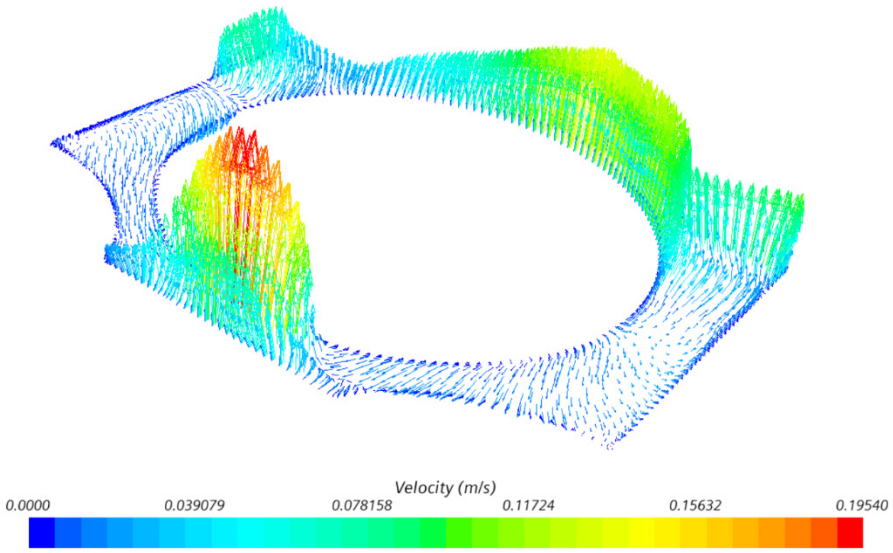

Figure 16 Velocity vector field in the cylinder liner coolant jacket

STAR CCM+ offers several turbulence models. The K-epsilon turbulence model provides a good compromise between robustness, accuracy, and computational time. It has become the most widely used model for industrial applications and various forms of the model is available [7]. The K-epsilon model was also used in two similar studies that simulated the cooling system and thermal map of an engine [28] [29]. The models solve the transport equations for the turbulent dissipation rate and the turbulent kinetic energy to determine the turbulent eddy viscosity [7]. The most suitable version for this simulation seems to be the Realizable Two-Layer K-Epsilon with all y^+ wall treatment, which can be used with fine meshes that resolve the viscous sublayer. It works well with both low and high Reynolds number type meshes ($y^+\sim$ 1 and $y^+ > 30$).

Two turbulence properties must be specified for the coolant inlet and outlet when using the K-epsilon turbulence model. One is the turbulence intensity I, which is the ratio of characteristic turbulent eddy velocity to the free stream velocity. The other is the turbulent length scale ℓ, which is a characteristic length scale of the energy-containing turbulent eddies [3]. The turbulence intensity and turbulent length scale are used to calculate the turbulent kinetic energy K and the turbulent dissipation rate (epsilon). K and epsilon can be specified directly at the inlet and outlet. However, appropriate values are not always known, and it is often more useful to specify I and ℓ. A rule of thumb is to use 0.1 for the turbulence intensity and half of a characteristic length for the turbulent length scale [3]. A value of 5 mm, which is half of the coolant jacket thickness around the cylinder liner, is used for the turbulent length scale and 0.1 is used for the turbulence intensity in the simulation.

The material used for the solid region of the engine is grey cast iron with a thermal conductivity of $53\ \frac{W}{m\,K}$ and density of $7870\ \frac{kg}{m^3}$. The material and fluid properties are assumed to be isotropic with constant density.

An internal combustion engine can be analyzed as a steady state system where energy enters and leaves the system at a steady rate. Energy enters the system with the fuel and leaves the system as heat, increased exhaust enthalpy, and shaft work. The heat transfer can also be considered steady for most cases as discussed in chapter 2.3.1, and the steady state time model is therefore used in this simulation [38]. The physics models used for the simulations are summarized in Table 9.

Table 9 Physics models

Turbulent	Liquid single-phase
Realizable K-Epsilon Two-Layer	Segregated Solid Energy
All y^+ wall treatment	Segregated Fluid Temperature
Segregated Flow	Solution Interpolation

4. Results and Discussion

There are several values that can be used to verify that the simulations are successful. The first is to check the residual values. Residuals are calculated in each cell for all the governing equations, and it represents the degree to which the discretized governing equations are satisfied [7]. The residual plot for the reference simulation is shown in Figure 17. It shows that the residuals are dropping by several orders of magnitude and that they are converging well. Similar plots are also seen for the nanofluid simulations.

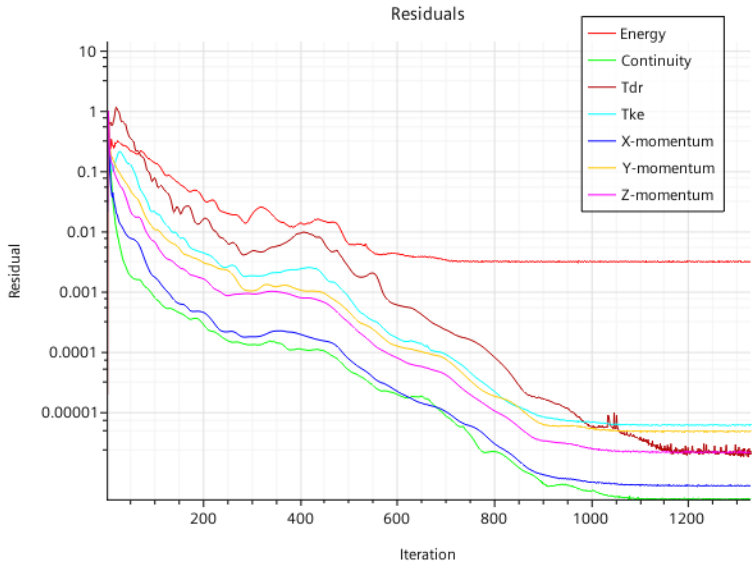

Figure 17 Residuals plot for the reference simulation

Residuals are useful for judging convergence of a solution. However, residuals have their limitations, and they cannot be relied upon as the only measure of convergence [7]. Other ways to determine convergence can be to monitor quantities of engineering interest (e.g., temperatures, mass flow rates, pressures, energy). The coolant outlet temperature settled at 80.9 °C for both the reference and 2.5 % CB simulation and it settled at 81.1 °C for the 10 % CB simulation. The dissipated heat due to convection and radiation from the outer surfaces of engine was 211 W for all the simulations. The energy transferred to the coolant was calculated by equation (31), where $\dot{m}$ is the coolant mass flow, c_p is the specific heat capacity of the fluid and $(T_{out} - T_{in})$ is the temperature difference between the inlet and outlet.

$$\dot{E} = \dot{m} c_p (T_{out} - T_{in}) \quad (31)$$

The results show that 3188 W was transferred to the coolant in all simulations. Combined with the heat dissipated from the outer surfaces it equals the total applied heat source which was 3399 W. All this information combined, indicate that the solution has converged well.

4.1. Flow Velocity

The general flow path and velocity of the coolant is almost identical for all simulations. General observations about the flow pattern regardless of coolant is thus presented here together. Figure 18 shows the flow pattern with streamlines, where the color of the streamline indicates the velocity. The black lines illustrate the paths with highest velocity and where the bulk fluid is flowing.

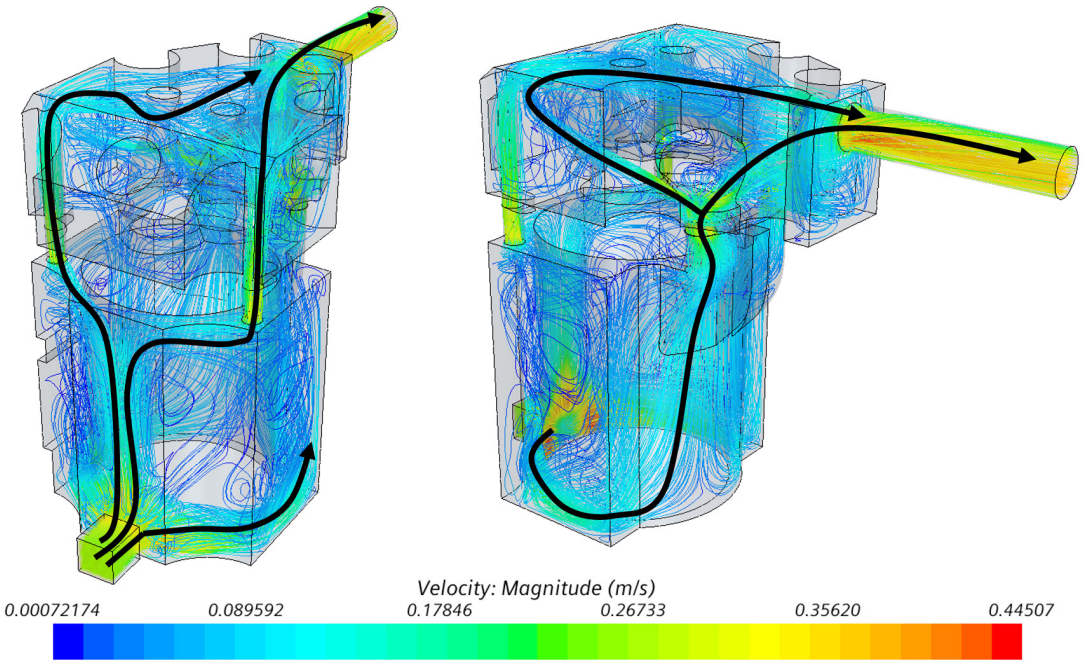

Figure 18 Flow velocity streamlines

Flow velocity at the walls of the fluid region is shown in Figure 19. The figure on the left has a velocity scale from 0 up to the maximum velocity of 0.37 m/s, while the figure on the right only shows velocities up to 0.05 m/s and everything above that is colored red. This is done for better visualization of the regions with low flow velocity. The black circles in Figure 19 shows areas with very low flow velocity and thus poor heat transfer. Both Figure 18 and Figure 19 shows

that the flow velocity is much higher at the front and rear of the cylinder liner compared to the right and left side.

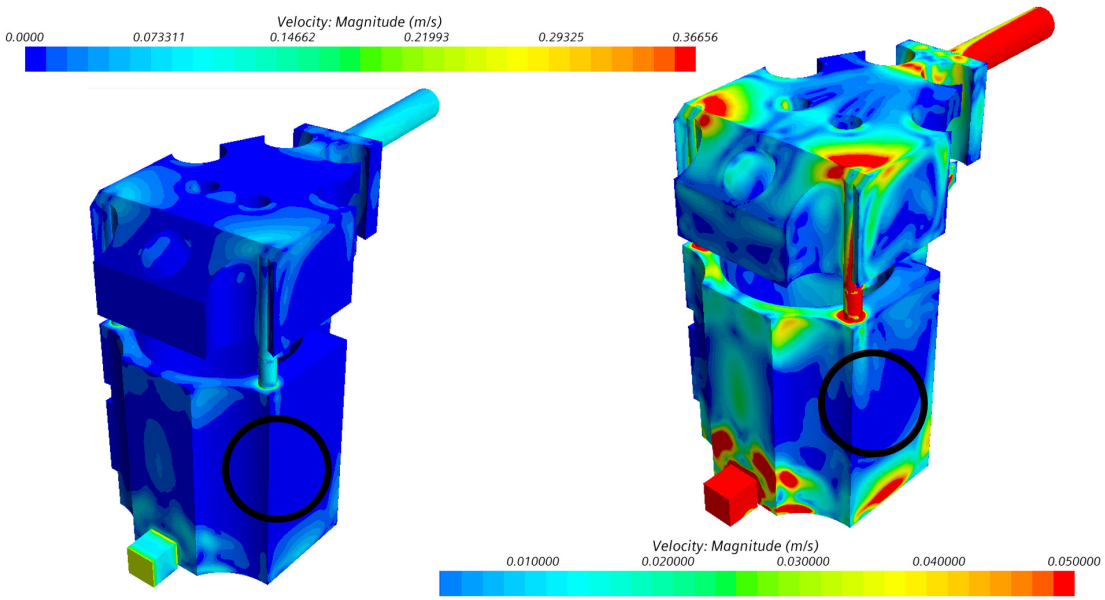

Figure 19 Flow velocity

The area with low flow velocity is also present on the coolant side of the cylinder liner as shown with the black circle in Figure 20. The left side of Figure 20 shows the coolant that surrounds the top of the combustion chamber with the injector and valves. The flow velocities in this area are also low.

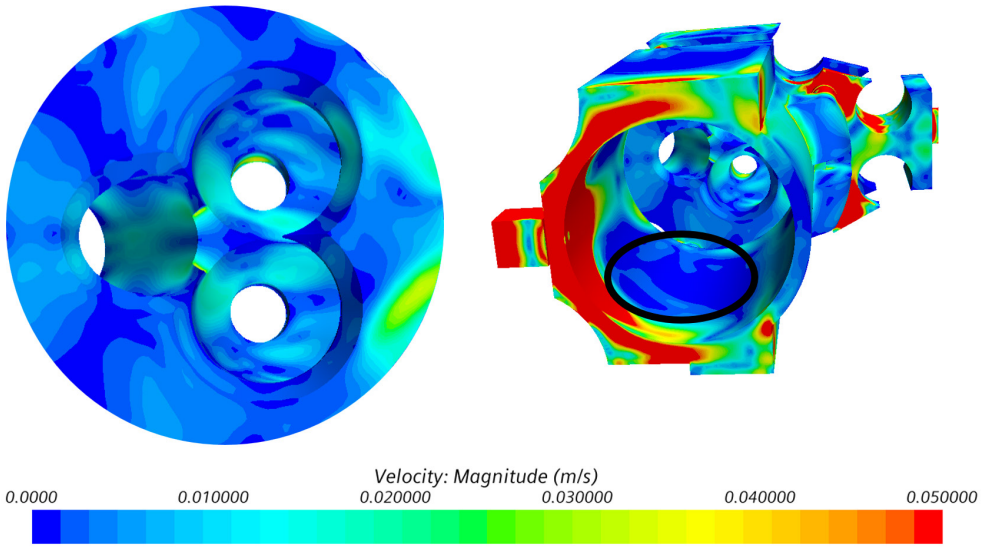

Figure 20 Liner and head flow velocity

4.2. Heat Transfer and Temperature Distribution

Temperature distribution in the solid region when switching between the different coolants is almost indistinguishable, as it was with the flow velocity. Figure 21 shows the temperature distribution of the solid region from the reference simulation with water as coolant. The equivalent figures for the nanofluid simulations are almost identical, hence they are not shown here. From the figure of the temperature distribution, it is possible to see that the highest temperatures on the cylinder liner occurs at the same locations where the coolant flow rate is lowest, which is the left and right side of the liner. It is also possible to see that the temperatures at the top of the combustion chamber are high, which makes sense due to the low flow velocities in that area.

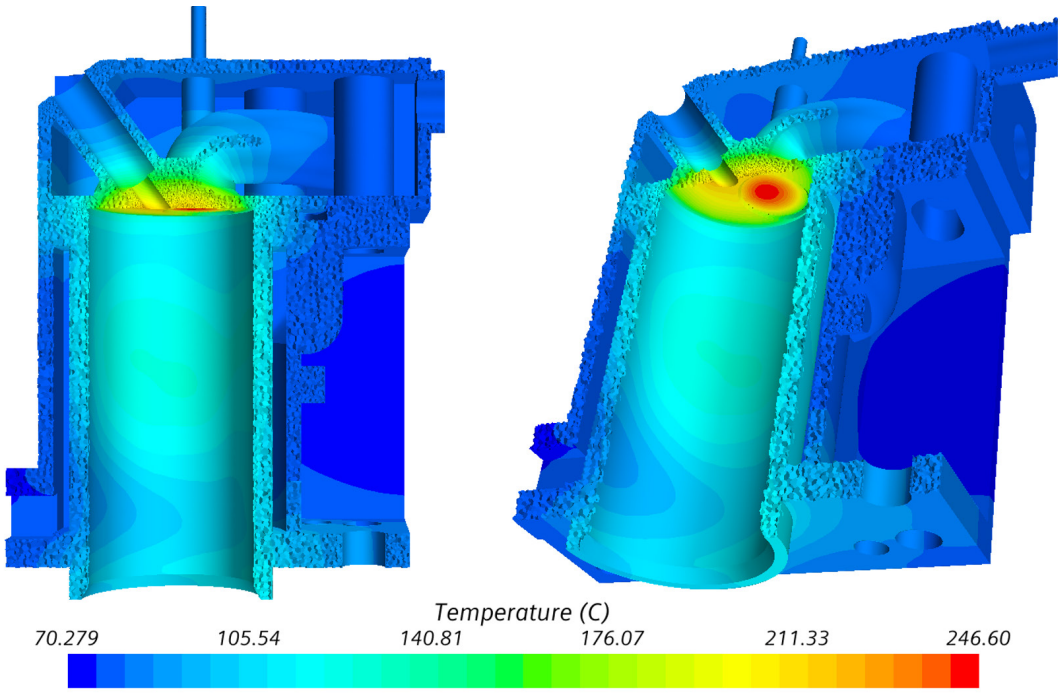

Figure 21 Reference simulation temperature distribution

Temperature reports for various surfaces was set up to quantify the difference between the coolants. The most relevant surfaces are the ones facing the combustion chamber and the coolant side of the cylinder liner. Table 10 shows the average and maximum temperatures for the surfaces. Results show that temperatures are higher on all these surfaces when using nanofluids, with the 10 wt% CB nanofluid being the worst performer. This is probably due to a large increase in viscosity (150%) relative to the increase in conductivity (15%) compared to water.

Table 10 Surface temperature comparison, water and nanofluid

	Water	**2.5% CB**	**10% CB**
Liner gas side avg. temp. [°C]	**112.4**	113.5	116.5
Liner gas side max. temp [°C]	**130.0**	131.3	133.4
Liner coolant side avg. temp. [°C]	**106.4**	107.2	110.7
Liner coolant side max. temp [°C]	**121.4**	121.8	128.1
Head gas side avg. temp. [°C]	**190.4**	191.5	193.0
Head gas side max. temp [°C]	**246.8**	246.8	248.2

The carbon-black nanofluid properties from the master thesis by S. Ruud [35] shows a decrease in heat transfer compared to water. Therefore, it was decided to try other types of nanofluids in the simulation with values obtained from other studies. A best-case scenario simulation was performed with nanofluid properties obtained from an experimental study [21]. The study discusses the viscosity, thermal conductivity, and heat transfer of nanofluids. Experimental data from tests of many different nanofluids are also presented. This best-case simulation uses a water-based nanofluid with 150 nm aluminum oxide (Al_2O_3) nanoparticles at a volume concentration of 2 %. The relative thermal conductivity and relative viscosity compared to the base-fluid is 1.13 and 1.134 respectively. Table 11 shows the properties of the best-case nanofluid, where the conductivity and viscosity are calculated from the values of water at 75 °C multiplied by the relative coefficients from the experimental study. The specific heat capacity and density is calculated by equation (20) and (21) from chapter 2.4.

Table 11 Properties of 2 % Al_2O_3 nanoparticles with water as base-fluid

		Relative to water
Coolant type	Water-based Al_2O_3 nanofluid	
Particle size	150 nm	
Temperature	75 °C	
Specific Heat Capacity c_p	3939 J/kg·K	0.94
Conductivity k	0.754 W/m·K	1.13
Density ρ	1035 kg/m^3	1.06
Dynamic Viscosity μ	0.429 mPa·s	1.134

Results from the best-case simulation show that temperatures are 1-2 °C lower on all the surfaces when using 2 % Al_2O_3 nanofluid compared to water. The bar chart in Figure 22 show temperature on the liner surfaces for water and the three nanofluids. It illustrates that the 2 % Al_2O_3 nanofluid shows better heat transfer properties in this simulation.

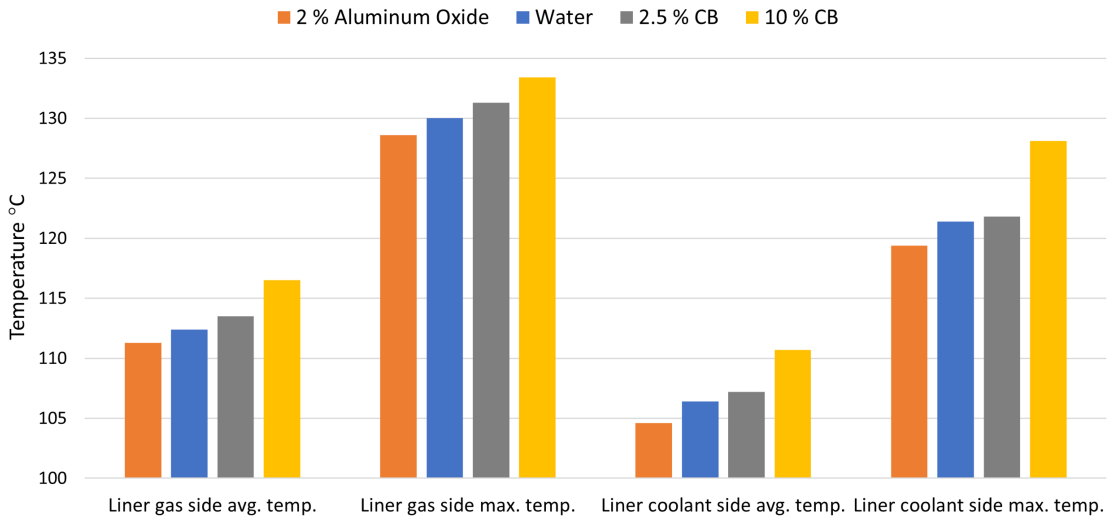

Figure 22 Surface temperature comparison between water and nanofluids

4.3. General Comments

The observed decrease in heat transfer with the carbon black nanofluids was not unexpected, as the increase in viscosity was relatively large compared to the increase in thermal conductivity. Similar results are observed in a study by Pak and Cho, who studied turbulent flow of Al_2O_3 and TiO_2 nanoparticles using water as base fluid in a circular pipe experimentally. The results showed that with a 3% volume concentration of Al_2O_3 nanoparticles the heat transfer coefficient was about 12 % less than with pure water. The result was attributed to a significant increase in the viscosity of the nanofluid which cancelled out the effect of improved conductivity [39].

A challenge with the simulations performed in this thesis is that CFD software is generally not good at simulating fluid flow that is in the laminar/turbulent transition phase, which is the case here [5]. This can possibly lead to results that does not match well with reality. Another possible cause of error is that the thermal conductivity is constant, meaning that the effect of Brownian motion and temperature change is neglected in the simulations.

The difference in surface temperature between the coolants are only a couple of degrees Celsius, which could be due to an unsuitable turbulence model for the nanofluids, or any other parameter which suits water better than the nanofluids. Experimental tests should be performed to determine if the results from the simulations represent an accurate portrayal of reality.

5. Conclusion

The use of water-based nanofluids with carbon black nanoparticles as coolant in a single-cylinder diesel engine was studied. A 3D model of the engine was created, and numerical simulation software was used to determine the temperature distribution in the engine. Three different nanofluids were tested and water was used as the reference point. The water-based carbon black nanofluids had a particle concentration of 2.5 and 10 weight percent with a particle size of 50 nm. An additional nanofluid was also tested, which was a water-based nanofluid with 2 % aluminum oxide nanoparticles with a size of 150 nm. The aluminum oxide nanofluid had a better relative increase in thermal conductivity and viscosity compared to the carbon black nanofluids and was thus used as a best-case scenario.

The results show that the average and maximum surface temperatures on selected surfaces in the engine are generally 1 to 4 °C higher with the carbon black nanofluids compared to the reference simulation with water. The aluminum oxide nanofluid achieved temperatures that were 1 to 2 °C lower than the reference simulation, thereby indicating improved heat transfer.

The findings indicate that the increase in viscosity negates the effect from the increased thermal conductivity of the nanofluid. The carbon black nanofluids tested in this thesis result in higher surface temperatures in the engine and therefore also a decrease in heat transfer coefficient compared to the base-fluid water. However, the temperature difference that is observed is relatively small and could be due to unknown errors or other uncertainties. Experimental tests should be performed to verify the result from the simulations and to see if the model is a good representation of reality.

5.1. Future Work

- Validate the 3D CFD simulation with experimental temperature data. This can be done by extensive instrumentation of the engine with temperature sensors that can be placed in strategic positions. The experimental results can then be compared with the results from the CFD simulation.
- Create a 3D combustion simulation to accurately model the heat flux and the spatial temperature distribution in the combustion chamber. This can enable the CFD simulation to accurately determine the temperature distribution in the engine.
- Continue work on the 1D engine simulation with updated experimental data. This could create an accurate model of the engine that can be used to simulate different operating modes like dual-fuel operation.
- The nanofluids could be further tested in an experimental test rig. A CFD model could also be made of the experimental setup and the results could then be compared.

6. Literature

[1] N. A. Che Sidik, M. N. A. M. Yazid and R. Mamat, "Recent advancement of nanofluids in engine cooling system," Renewable and Sustainable Energy Reviews 75 (137-144), 2017.

[2] G. Cicalese, F. Berni and S. Fontanesi, "Integrated In-Cylinder / CHT Methodology for the Simulation of the Engine Thermal Field: An Application to High Performance Turbocharged DISI Engines," SAE International, 2016.

[3] Y. A. Cengel and J. M. Cimbala, Fluid Mechanics: Fundamentals and Applications Fourth Edition, McGraw-Hill Education, 2020.

[4] K. Brautaset, Innføring i oljehydraulikk, Universitetsforlaget, 1983.

[5] "Realis WAVE User Manual Version 2022.3," Realis Simulation Inc., 2022.

[6] J. Blazek, Computational Fluid Dynamics: Principles and Applications, Elsevier Ltd., 2005.

[7] "Simcenter STAR-CCM+ 2020.1 Manual," Siemens, 2020.

[8] J. B. Heywood, Internal Combustion Engine Fundamentals Second Edition, McGraw-Hill Education, 2018.

[9] Y. A. Cengel, M. A. Boles and M. Kanoglu, Thermodynamics An Engineering Approach ninth edition, McGraw-Hill Education, 2020.

[10] R. Stone, Introduction to Internal Combustion Engines second edition, The MacMillan Press LTD, 1992.

[11] G. Woschni, "A Universally Applicable Equation for the Instantaneous Heat Transfer Coefficient on the Internal Combustion Engine," SAE Transactions, Vol 76, Section 4: Papers 670805-670984, pp. 3065-3083, 1968.

[12] G. F. Hohenberg, "Advanced Approaches for Heat Transfer Calculations," SAE Transactions, Vol 88, Section 3, pp. 2788-2806, 1979.

[13] L. Fonseca, P. Olmeda, R. Novella and R. M. Valle, "Internal Combustion Engine Heat Transfer and Wall Temperature Modeling: An Overview," Archives of Computational Methods in Engineering 27:1661-1679, 2019.

[14] K. Mollenhauer and H. Tschoeke, Handbook of Diesel Engines, Springer, 2010.

[15] F. W. Dittus and L. M. Boelter, "Heat transfer in automobile radiators of the tubular type," University of California Publications in Engineering, vol. 2, p. 443, Berkeley, 1930.

[16] J. Buongiorno, "Convective Transport in Nanofluids," ASME Vol. 128, March 2006, 2006.

[17] D. C. Venerus, J. Buongiorno and R. Christianson, et al., "Viscosity Measurements on Colloidal Dispersions (Nanofluids) for Heat Transfer Applications," Appl. Rheol. 20 44582, 2009.

[18] J. Eastman., et al., "Anomalously Increased Effective Thermal Conductivities of Ethylene-Glycol Based Nanofluids Containing Copper Nanoparticles," Applied Physics Letter 78(6), pp. 718-720, 2001.

[19] S. Das., et al., "Temperature Dependence of Thermal Conductivity Enhancement for Nanofluids," Journal of Heat Transfer, 125, pp. 567-574, 2003.

[20] Y. Xuan and W. Roetzel, "Conceptions for Heat Transfer Correlation of Nanofluids," International Journal of Heat Mass Transfer, 43, pp. 3701-3707, 2000.

[21] V. Rudyak and A. Minakov, "Thermophysical properties of nanofluids," The European Physical Journal E 41: 15, 2018.

[22] A. Minakow, V. Rudyak and M. Pryazhnikov, "Systematic Experimental Study of the Viscosity of Nanofluids," Heat Transfer Engineering Vol. 42, No. 12, 1024-1040, 2021.

[23] M. H. Buschmann, R. Azizian and T. Kempe, et al., "Correct interpretation of nanofluid convective heat transfer," International Journal of Thermal Sciences 129 (2018) 504-531, 2018.

[24] I. Behroyan, P. Ganesan and S. Sivasankaran, "Turbulent forced convection of Cu-water nanofluid: CFD model comparison," International Communications in Heat and Mass Transfer, 2015.

[25] J. Koo and C. Kleinstreuer, "A new thermal conductivity model for nanofluids," Journal of Nanoparticle Research 6:577-588, 2005.

[26] Z. Haddad, E. Abu-Nada, H. Oztop and A. Mataoui, "Natural convection in nanofluids: Are the thermophoresis and Brownian motion effects significant in nanofluid heat transfer enhancement?," International Journal of Thermal Sciences, 2011.

[27] S. Fontanesi, G. Cicalese, A. D'Adamo and G. Pivetti, "Validation of a CFD methodology for the Analysis of Conjugate Heat Transfer in a High Performance SI Engine," SAE Technical Paper, 2011.

[28] G. Cicalese, F. Berni, S. Fontanesi, A. D'Adamo and E. Andreoli, "A Comprehensive CFD-CHT Methodology for the Characterization of a Diesel Engine: form the Heat Transfer Prediction to the Thermal Field Evaluation," SAE Technical Paper 2017-01-2196, 2017.

[29] O. Iqbal, K. Arora and M. Sanka, "Thermal Map of an IC Engine via Conjugate Heat Transfer: Validation and Test Data Correlation," SAE International, 2014.

[30] *Petter Diesel PH1W Manual,* Lister Petter.

[31] K. Skaar, "Implementering av indikeringssytem på dieselmotor og tester av dieseloljer," University of Bergen, Master thesis, 2016.

[32] J. Tingstad, "Tilpasning av elektronisk innsprøytningssystem, type Common Rail, for en èn-sylindret dieseldrevet laboratoriemotor," University of Bergen, Master Thesis, 2017.

[33] M. H. Howarth, The Design of High Speed Diesel Engines, London: Constable, 1966.

[34] P. Flynn and S. K. Chen, "Development of a compression ignition research engine," SAE Paper 650733, 1965.

[35] S. G. Ruud, "Nanofluids for direct cooling application in a diesel engine," University of Bergen, Master thesis, 2023.

[36] VDI Heat Atlas Second Edition ISBN 978-3-540-77876-9, Springer Heidelberg Dordrecht London New York, 2010.

[37] M. N. Ozisik, Heat Transfer - A Basic Approach, McGraw-Hill, 1985.

[38] S. Qin and C. Xie., et al., "CFD Analysis and Optimization of a Diesel Engine Cooling Water Jacket," Fluid Dynamics & Materials Processing, 2021.

[39] B. C. Pak and Y. I. Cho, "Hydrodynamic and Heat Transfer Study of Dispersed Fluids with Submicron Metallic Oxide Particles," Experimental Heat Transfer, 11, pp. 151-170, 1998.

[40] C. F. Taylor, The Internal Combustion Engine in Theory and Practice, Volume 1: Thermodynamics, Fluid Flow, Performance., Cambridge: The M.I.T. Press, 1985.

[41] A. Sanli, A. N. Ozsezen, I. Kilicasland and M. Canakci, "The influence of engine speed and load on the heat transfer between gases and in-cylinder walls at fired and motored conditions of an IDI diesel engine," Applied Thermal Engineering 28 (2008) 1395-1404.

[42] E. G. Pariotis, G. M. Kosmadakis and C. D. Rakopoulos, "Comparative analysis of three simulation models applied on a motored internal combustion engine," Energy Conversion and Management 60, 45-55, 2012.

Attachment 1

Measurement data from test run at 1500 rpm 30 Nm [32]

Torque [Nm]	**14.90**	**29.82**
Speed [1/min]	1500.50	1500.25
Ambient air temperature [°C]	26.98	27.00
Exhaust temperature [°C]	310.23	522.85
Fuel consumption [kg/h]	0.77	1.37
Indicated mean effective pressure [bar]	4.09	7.12
Pmax [bar]	65.29	75.70
Start of injection	26° BTDC	26° BTDC
Start of combustion	7.5° BTDC	9° BTDC

Attachment 2

Data from Petter Diesel PH1W manual [30]

Power at 2000 rpm [kW]	6.15
Power at 1500 rpm [kW]	4.7
Compression ratio	16.5: 1
Fuel injection timing at 1500 rpm	24° BTDC
Inlet valve opens	4.5° BTDC
Inlet valve closes	35.5° ABDC
Exhaust valve opens	35.5° BBDC
Exhaust valve closes	4.5° ATDC
Bore [mm]	87,3
Stroke [mm]	110
Compression pressure [bar]	36.88
Firing pressure at max load [bar]	72.39
Brake thermal efficiency [%]	32

Attachment 3

1D Engine Simulation Inputs

Speed [1/min]	1500
Torque [Nm]	29.82
Ambient air temperature [°C]	27.00
Strokes per cycle	4
No. of cylinders	1
Bore [mm]	87.3
Stroke [mm]	110
Compression ratio	16.5: 1
Combustion model	Diesel Wiebe Combustion
Convective heat transfer	Original Woschni
Friction model	Chen-Flynn friction
Piston volume [mm^3]	239 400
Piston coolant-side area [mm^2]	5 985
Head volume [mm^3]	1 261 526
Head coolant-side area [mm^2]	(Whole inside area 98 083) / 30 417
Head wall thickness [mm]	7
Liner volume [mm^3]	674 477
Liner coolant-side area [mm^2]	51 095
Liner wall thickness [mm]	9.85
Coolant temperature [°C]	75
Material	Grey cast iron
Material conductivity [W/m K]	53
Head heat transfer coefficient [W/m^2 K]	1433
Liner heat transfer coefficient [W/m^2 K]	1518
Start of injection	26° BTDC
Start of combustion	9° BTDC

Attachment 4

Free Convection from Engine Block

The free convection heat transfer from the outer surface of the engine block is calculated by the methodology described in VDI Heat Atlas chapter F1 [36] (Boussinesq approximation). The methodology can be summed up in four steps:

1. Determine a reference temperature T_*, and compile the fluid properties shown in Table 12.
2. Compute the nondimensional Rayleigh (Ra) and Prandtl number (Pr).
3. Compute the Nusselt number $Nu(Ra, Pr)$.
4. Compute the convective heat transfer coefficient $h_c(Nu, \lambda, L)$.

$$Nu = 5.748 + 0.752 \left(\frac{Ra}{f_4(Pr)}\right)^{0.252} \tag{32}$$

$$f_4(Pr) = \left(\left(1 - \frac{0.492}{Pr}\right)^{9/16}\right)^{16/9} \tag{33}$$

$$Ra = \frac{\beta g \Delta T L^3}{va} \tag{34}$$

The reference temperature T_* is calculated by equation (35). With $T_{surface}$ as the surface temperature of the engine block (80 °C) and T_∞ as the ambient air temperature (20 °C), T_* becomes 50 °C.

$$T_* = \frac{1}{2} \cdot (T_{surface} + T_\infty) \tag{35}$$

The properties of air at 50 °C are listed in Table 12.

Table 12 Properties of air at 50 °C

Density ρ	$1.0779\ kg/m^3$
Kinematic viscosity ν	$182.2 \cdot 10^{-7}\, m^2/s$
Thermal diffusivity a	$258.54 \cdot 10^{-7}\, m^2/s$
Isobaric volume expansion coefficient β	$3.1010 \cdot 10^{-3}\, 1/K$
Prandtl number Pr	0.7045
Thermal Conductivity λ	$0.028082\ W/m\,K$

The engine block has a cube like shape with a characteristic length L as shown in equation (36), which gives a characteristic length of 1.502 meters.

$$L = \frac{Area^2}{4 \cdot Volume} \tag{36}$$

Inserting the properties from Table 12 into equation (32), (33), and (34) results in a Nusselt number of 350.3. The convective heat transfer coefficient is given by equation (37), and by inserting the Nusselt number, thermal conductivity, and characteristic length, $h_{convection}$ becomes 6.6 W/m^{2}K.

$$h_{convection} = \frac{Nu \cdot \lambda}{L} \tag{37}$$